

SYMMETRIES AND PATTERN SELECTION IN RAYLEIGH–BÉNARD CONVECTION

M. GOLUBITSKY

Department of Mathematics, University of Houston, Houston, Texas 77004, USA

and

J.W. SWIFT and E. KNOBLOCH

Department of Physics, University of California, Berkeley, California 94720, USA

Received 10 May 1983

Revised 29 June 1983

This paper describes the process of pattern selection between rolls and hexagons in Rayleigh–Bénard convection with reflectional symmetry in the horizontal midplane. This symmetry is a consequence of the Boussinesq approximation, provided the boundary conditions are the same on the top and bottom plates. All possible local bifurcation diagrams (assuming certain non-degeneracy conditions) are found using only group theory. The results are therefore applicable to other systems with the same symmetries. Rolls, hexagons, or a new solution, regular triangles, can be stable depending on the physical system. Rolls are stable in ordinary Rayleigh–Bénard convection. The results are compared to those of Buzano and Golubitsky [1] without the midplane reflection symmetry. The bifurcation behavior of the two cases is quite different, and a connection between them is established by considering the effects of breaking the reflectional symmetry. Finally, the relevant experimental results are described.

1. Introduction

Rayleigh–Bénard convection provides perhaps the best studied example of nonlinear pattern selection. In the simplest version of the problem a layer of fluid confined between infinite, stress-free, horizontal boundaries is heated uniformly from below. For small temperature differences, measured by the Rayleigh number R , energy is transported by molecular conduction. As R is increased, the conduction state loses stability. At $R = R_c$, the point of neutral stability, the linear stability problem admits several qualitatively different planforms: rolls, squares, hexagons, and in fact any linear combination of rolls with the critical wavelength. For supercritical values of R the amplitude of each planform grows exponentially until the nonlinear effects become important. The nonlinear terms are responsible for selecting one of the patterns admitted by the linearized problem. In the laboratory, this process will be affected by random

initial conditions and imperfections in the apparatus, as well as by the presence of sidewalls, all of which will have an effect on pattern selection.

Much theoretical work on convection assumes the Boussinesq approximation, in which all material properties are independent of temperature, with the exception of the density entering in the driving buoyancy term. If, in addition, the boundary conditions are the same on the top and bottom plates, and the mean temperature in the layer is time-independent [2], then the resulting problem is symmetric under a reflection in the horizontal midplane, together with a temperature reversal. Under such conditions it has been predicted (Schlüter et al. [3]) that in a large aspect ratio container rolls will be observed at the onset of convection. On the other hand, in systems lacking the reflectional symmetry, i.e., non-Boussinesq fluids, or systems with asymmetrical boundary conditions or time-dependent heating, hexagons are usually observed. This tendency has been explained for a

number of specific systems (see, for example, the review by Busse [4]). On the other hand, it is evident that it is the basic symmetry differences that are responsible for the observed results. In this paper we present a method that takes full advantage of the symmetries of the problem, and are able to give a complete classification of all possible steady state bifurcations near onset that are consistent with the imposed symmetries and certain nondegeneracy conditions. In particular, we clarify the nature of the transition between hexagons and rolls as the Rayleigh number is increased, and between rolls and hexagons as the reflectional symmetry is broken.

The convection problem has traditionally been treated using perturbation expansions. The method has yielded many interesting and valuable results that are summarized by Busse [4]. Standard perturbation expansions suffer from two disadvantages, however; first, they do not take full advantage of the various symmetries of the problem. Consequently, it is often unclear which aspects of the solutions are a consequence of the symmetries, and hence, which class of problems will exhibit the same dynamics. Second, perturbation expansions are carried out to some order, and the higher order terms are neglected without adequate justification. For example, existing calculations [4] are restricted to third order in the amplitude of the instability. The basic issue here is: to what order must an expansion be taken if the addition of higher order terms is not to change any qualitative aspects of the dynamics. Results of this kind are called structural stability results.

The proof of structural stability for vector fields in dimensions ≥ 3 is, however, almost impossible [5]. In the present paper we therefore restrict attention to stationary solutions whose bifurcation structure can be studied rigorously by means of either singularity theory or group theory. For the present problem, the latter is easier to apply. Moreover, it highlights the role played by the symmetries in determining both the possible bifurcating solution branches and their stability properties. For example, we are able to classify the

bifurcating solutions by their symmetries. The group of symmetries of a given solution is called the *isotropy subgroup*. It is a subgroup of the group of symmetries of the problem. We find that the solutions that bifurcate off the trivial conduction solution are those whose symmetry is described by *maximal* isotropy subgroups of the group of symmetries of the trivial solution, i.e., the next most symmetric solutions.

The equations describing Rayleigh–Bénard convection in the Boussinesq approximation are

$$\frac{1}{P} \left[\frac{\partial \mathbf{u}}{\partial t} + (\mathbf{u} \cdot \nabla) \mathbf{u} \right] = -\nabla p + \theta \hat{y} + \nabla^2 \mathbf{u}, \quad (1.1a)$$

$$\frac{\partial \theta}{\partial t} + \mathbf{u} \cdot \nabla \theta = R w + \nabla^2 \theta, \quad (1.1b)$$

$$\nabla \cdot \mathbf{u} = 0, \quad (1.1c)$$

where $\mathbf{u} = (u, v, w)$ in the velocity relative to (x_1, x_2, y) directions, and θ denotes the departure from a linear temperature profile. The dimensionless numbers R and P are, respectively, the Rayleigh and Prandtl numbers. For the analysis that follows, it is important to understand the symmetry properties of these equations and the behavior of the linear eigenfunctions under the symmetries. Also of importance is the fact that there is a critical wavenumber k_c which first goes unstable as the Rayleigh number is increased. The explicit equations (1.1) will not be required, however.

The equations of motion must be supplemented with appropriate boundary conditions. We are interested in studying the role played by the boundary conditions on the upper and lower plates, but will assume that the lateral boundaries are sufficiently far away that the fluid layer can be considered infinite in both horizontal directions. The convection equations are then equivariant with respect to rigid motion in the plane. The onset of convection is an example of a symmetry breaking bifurcation. The crucial simplifying assumption we make is that the resulting pattern is doubly

periodic in the horizontal plane, i.e., that there are two translation vectors a_1, a_2 in the horizontal plane such that the functions $f(x)$ in the plane that we will allow satisfy

$$f(x) = f(x + n_1 a_1 + n_2 a_2) \tag{1.2a}$$

for all integers n_1, n_2 . The Fourier transform of such a doubly periodic function is discrete:

$$f(x) = \sum_{m_1, m_2} z_{m_1 m_2} e^{i(m_1 k_1 + m_2 k_2)}, \quad z_{-m_1, -m_2} = \bar{z}_{m_1, m_2}, \tag{1.2b}$$

where the reciprocal space vectors $k_\beta (\beta = 1, 2)$ are related to the spatial translations $a_\alpha (\alpha = 1, 2)$ by

$$a_\alpha \cdot k_\beta = 2\pi \delta_{\alpha\beta}. \tag{1.2c}$$

In the following we shall assume that the vectors k_α have a length equal to the critical wavenumber k_c at the onset of instability. The resulting k -space lattice is either square, rhombic, or hexagonal. Sattinger [6] has studied these cases but without considering the effects of the midplane reflectional symmetry; this symmetry has, however, important consequences for the hexagonal lattice. Moreover, the most frequently observed convection patterns, rolls and hexagons, are both doubly periodic with respect to the hexagonal lattice, although squares are sometimes seen. The observed patterns are, however, rarely stationary and defect free (see, for example Koschmieder [7]).

For these reasons we restrict our attention to patterns which are doubly periodic with respect to the hexagonal lattice. Fig. 1a shows the translation vectors a_1, a_2 and three copies of the hexagonal unit cell. The pattern in each cell is repeated so as to tile the whole plane. Fig. 1b shows the longest wavelength rolls that have the required double periodicity. Fig. 1c shows the 6 points of the k -space lattice which are assumed to have the critical wavenumber. Note that it is possible that 12 (or more) points of the k -space lattice intersect the circle of critical wavenumbers, as in fig. 1d where

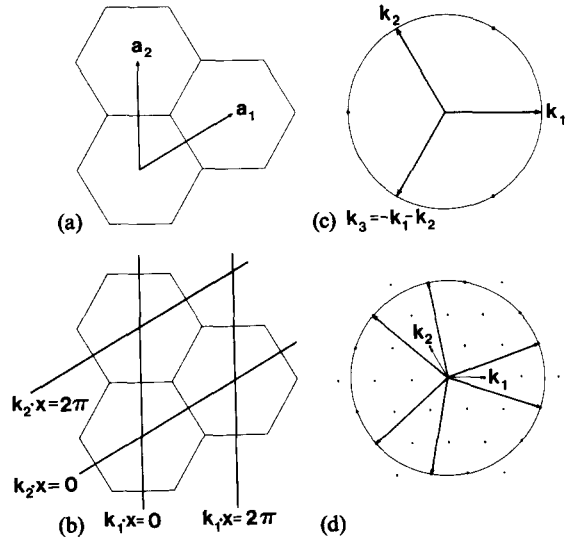


Fig. 1. Doubly-periodic functions in the plane and the hexagonal lattice: (a) unit cells and translation vectors, (b) rolls on the hexagonal lattice, and (c, d) the circle of critical wavevectors intersecting 6 or 12 modes on the reciprocal lattice.

$3k_1 + k_2$ is a critical mode. In this case the imposed spatial periodicity is larger than the wavelength of the instability.

Apart from the assumed symmetry with respect to translations on a hexagonal lattice, the equations are invariant under reflection in the midplane $y = 0$,

$$\begin{aligned} x' &= x, & (u', v') &= (u, v), \\ y' &= -y', & w' &= -w, & \theta' &= -\theta. \end{aligned} \tag{1.3}$$

If the boundary conditions at the two horizontal plates $y = \pm \frac{1}{2}$ are time-independent and identical, then the system has reflectional symmetry about $y = 0$. For stress-free, perfectly conducting boundaries, the eigengunctions of the linearized convection equations are

$$\begin{pmatrix} u \\ v \\ w \\ \theta \end{pmatrix}_{(k, n)} = \begin{pmatrix} A_1 \sin n\pi y \\ A_2 \sin n\pi y \\ iA_3 \cos n\pi y \\ iA_4 \cos n\pi y \end{pmatrix} e^{ik \cdot x}, \tag{1.4}$$

where the A_i are real constants, and k is the

wavevector in the horizontal (x) plane. The critical modes have $n = 1$ and $|k|^2 = k_c^2 = \pi/2$. Under the reflection (1.3) the eigenfunctions transform as

$$\begin{aligned} u'_{k,n}(x', y') &= (-1)^n u_{k,n}(x, y), \\ \theta'_{k,n}(x', y') &= (-1)^n \theta_{k,n}(x, y). \end{aligned} \tag{1.5}$$

The eigenfunctions of (1.1) always have this symmetry if the boundary conditions are symmetric.

The real (or imaginary) parts of the critical modes are called rolls (fig. 2a). The effect of the reflectional symmetry on a roll is to reverse the direction of the flow. Likewise, the symmetry transforms hexagons with the flow up in the middle (H^+) (fig. 2b) to hexagons with the flow down in the middle (H^-) (fig. 2d). With the reflectional symmetry, both types of hexagons are on an equal footing; if hexagons are stable, then either H^+ or H^- is the realized planform, depending on initial conditions. Moreover, in this case two new solutions, which we call regular triangles (fig. 2c) and

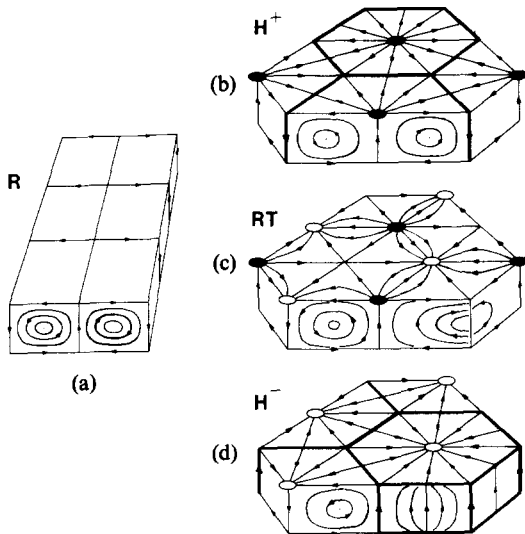


Fig. 2. Regular convection patterns: (a) rolls (R), (b) hexagons with flow up in the center and down along the sides (H^+), (c) regular triangles (RT), and (d) hexagons with flow down in the center and up along the sides (H^-). The patterns H^\pm and RT differ only in the phase Φ : $\Phi = 0$ (H^+), $\Phi = \pi/2$ (RT), $\Phi = \pi$ (H^-). Fig. 4 shows details of the transition between the hexagons and triangles.

the patchwork quilt (fig. 4a) exist near the instability. On the other hand, in problems without the reflectional symmetry these solutions do not occur near instability, and one type of hexagons or the other is preferred.

It is important to note that if the critical modes had been *even* rather than *odd* (e.g., n is even in eqs. (1.5)) then the symmetry would be “trivial”. By this we mean that only even modes are generated by the nonlinear coupling of the critical modes, and the symmetry is preserved by the finite amplitude solutions. In this case the results without the reflectional symmetry would be valid. The important, i.e., non-trivial, symmetries are those that are broken by the bifurcating solutions.

In studying the pattern selection problem on a hexagonal lattice with the midplane reflection, we complement the recent work of Buzano and Golubitsky [1] on the problem without the reflectional symmetry. In the following, we reinterpret the results of Buzano and Golubitsky and show that the bifurcation diagrams for the symmetric case are quite different. The group theory methods we use are explained in sections 2 and 3. In section 2 we present the classification of bifurcating solutions by their isotropy subgroups; the bifurcation diagrams are computed in section 3. In section 4, the results are compared with those of Buzano and Golubitsky on the nonsymmetric problem, and the breaking of the reflectional symmetry is discussed. The results are summarized in section 5 where a brief overview of the relevant experimental observations is provided.

2. Classification of the solutions

2.1. The amplitude equations

The assumption of double periodicity reduces the partial differential equations (1.1) to a set of coupled ordinary differential equations for the Fourier amplitudes of each field (cf. eq. (1.2b)). Thus, there is only a finite number of critical modes at the onset of instability ($R = R_c$), and the Center Manifold Theorem [8] justifies a description of the

dynamics near $R = R_c$ in terms of a finite number of amplitudes.

For a hexagonal lattice with 6 wavevectors on the circle of critical wavenumbers, we may write the temperature perturbation as

$$\theta(x, y, t) = \operatorname{Re} \left\{ \sum_{\alpha=1}^3 z_\alpha(t) e^{i\mathbf{k}_\alpha \cdot \mathbf{x}} f(y) \right\}, \quad (2.1)$$

where z_α ($\alpha = 1, 2, 3$) are complex amplitudes of the bifurcating modes, and $f(y)$ is the appropriate vertical eigenfunction. The \mathbf{k}_α are three of the critical wavevectors, each of magnitude k_c , and each oriented at 120° to the other two, so that $\mathbf{k}_1 + \mathbf{k}_2 + \mathbf{k}_3 = 0$ (cf. fig. (1c)).

We are assuming that each of the 6 modes goes unstable via a single eigenvalue passing through zero, and do not consider the Hopf bifurcations that can arise in some convection systems [9].

With these assumptions, the partial differential equations near the bifurcation reduce to three complex amplitude equations for the critical modes, of the form

$$\dot{z}_\alpha = g_\alpha(z_1, z_2, z_3, \lambda), \quad \alpha = 1, 2, 3, \quad (2.2)$$

where λ is the bifurcation parameter, proportional to $R - R_c$. The amplitude equations are symmetric (equivariant) with respect to the symmetry group Γ_n , the largest subgroup of the Euclidean group in the plane that preserves doubly periodic functions on a fixed hexagonal lattice, or the groups $\Gamma_s = \Gamma_n + Z_2$ when the midplane reflectional symmetry is included. We use the subscripts n and s on Γ to denote the nonsymmetric and symmetric cases, respectively. Let

$$z = (z_1, z_2, z_3), \quad g = (g_1, g_2, g_3).$$

The symmetry then implies

$$g(\gamma z, \lambda) = \gamma g(z, \lambda), \quad \text{for all } \gamma \text{ in } \Gamma_n \text{ or } \Gamma_s. \quad (2.3)$$

The allowed rotations and reflections form the group D_6 , the dihedral group of planar symmetries

of a hexagon. The translations are identified with the torus T^2 by the double periodicity. Thus $\Gamma_n = D_6 + T^2$, a semidirect product of D_6 and T^2 , implying that Γ_n consists of all 12 elements of D_6 composed with all translations.

The form of the amplitude equations is restricted by the requirement (2.3). To use (2.3) we first have to understand the action of Γ_n on $z = (z_1, z_2, z_3) \in C^3$. From eq. (2.1) translations $\mathbf{x} \mapsto \mathbf{x} + \mathbf{d}$ are described by the action $T^2 \times C^3 \rightarrow C^3$:

$$(s, t) \cdot z = (e^{is}z_1, e^{-i(s+t)}z_2, e^{it}z_3), \quad (2.4a)$$

where $s = \mathbf{k}_1 \cdot \mathbf{d}$ and $t = \mathbf{k}_3 \cdot \mathbf{d}$. The twelve rotations and reflections of D_6 are generated by D_3 , the symmetry group in the plane of an equilateral triangle, and inversion through the origin ($\mathbf{x} \mapsto -\mathbf{x}$) which induces the complex conjugation mapping

$$c: z \mapsto \bar{z} \quad (2.4b)$$

on C^3 . Moreover, D_3 is generated by rotation through 120° and reflection in a vertical plane:

$$\begin{aligned} r_{120^\circ}: (z_1, z_2, z_3) &\mapsto (z_2, z_3, z_1), \\ \sigma_v: (z_1, z_2, z_3) &\mapsto (z_1, z_3, z_2). \end{aligned} \quad (2.4c)$$

Finally, the midplane reflection (if it holds) changes the sign of the temperature variation and operates on C^3 by

$$\sigma_h: z \mapsto -z. \quad (2.4d)$$

The group Γ_n leaves unchanged the polynomials

$$\begin{aligned} \sigma_1 &= u_1 + u_2 + u_3, \\ \sigma_2 &= u_1u_2 + u_2u_3 + u_3u_1, \\ \sigma_3 &= u_1u_2u_3, \\ q &= z_1z_2z_3 + \bar{z}_1\bar{z}_2\bar{z}_3, \end{aligned} \quad (2.5)$$

where $u_\alpha = z_\alpha \bar{z}_\alpha$. It follows that any real-valued function $h = h(\sigma_1, \sigma_2, \sigma_3, q)$ is invariant under Γ_n .

As shown in Buzano and Golubitsky [1], all smooth functions invariant under Γ_n have this form. Moreover, it is also shown there that the equivariance condition (2.3) for Γ_n implies that the amplitude equations for the critical modes must have the form

$$\dot{z}_1 = z_1(h_1 + u_1 h_3 + u_1^2 h_5) + \bar{z}_2 \bar{z}_3 (p_2 + u_1 p_4 + u_1^2 p_6), \tag{2.6}$$

where h_j, p_j are λ -dependent invariant functions; that is, these functions depend on the 5 variables $\sigma_1, \sigma_2, \sigma_3, q, \lambda$. Equations for \dot{z}_2, \dot{z}_3 are obtained by cyclic permutation of z_1, z_2, z_3 . Note that $\bar{z}_2 \bar{z}_3$ transforms the same way as z_1 and that terms of the form $z_1 u_1^3$, etc., are not required since

$$u_1^3 = \sigma_3 - \sigma_2 u_1 + \sigma_1 u_1^2.$$

(The notation here is based on the choice of critical k -vectors $k_1 + k_2 + k_3 = 0$ and differs slightly from the notation in Buzano and Golubitsky where the critical k vectors were chosen to satisfy $k_1 - k_2 + k_3 = 0$.)

If the midplane reflection (2.4d) holds, only odd powers of z are allowed in the amplitude equations and the form of (2.6) is further restricted to

$$\dot{z}_1 = z_1(l_1 + u_1 l_3 + u_1^2 l_5) + \bar{z}_2 \bar{z}_3 q(m_5 + u_1 m_7 + u_1^2 m_9), \tag{2.7}$$

where l_j, m_j are now functions of $\sigma_1, \sigma_2, \sigma_3, q^2$, and λ .

2.2. Classification of the steady-state solutions

The solutions $z(\lambda)$ to the steady state equations $g(z, \lambda) = 0$ can be classified according to their symmetry. Since $g(\gamma z, \lambda) = \gamma g(z, \lambda)$, if z is a solution to $g(z, \lambda) = 0$, then so is the orbit of z , defined by

$$\Gamma z = \{\gamma z \mid \gamma \in \Gamma\}, \quad \Gamma = \Gamma_n \text{ or } \Gamma_s. \tag{2.8}$$

We consider all solution on an orbit to be equivalent. If an orbit is stable, then the actual solution

observed will depend on the initial conditions, since the equations treat all solutions on the orbit equivalently.

We classify the symmetry of a solution z by the isotropy group Σ_z , subgroup of Γ leaving z invariant,

$$\Sigma_z = \{\gamma \in \Gamma \mid \gamma z = z\}. \tag{2.9}$$

The other elements of the orbit Γz have isotropy groups related by conjugation. Thus, the symmetry of a solution γz is given by the conjugate subgroup $\gamma \Sigma_z \gamma^{-1}$ and one need only distinguish the conjugacy classes of isotropy subgroups when describing solutions.

In fig. 3 we list part of the lattices of isotropy subgroups for the representations of the groups Γ_n and Γ_s described by eqn. (2.4).

The most symmetric solution (the trivial or conduction solution) has isotropy subgroup Γ_n or

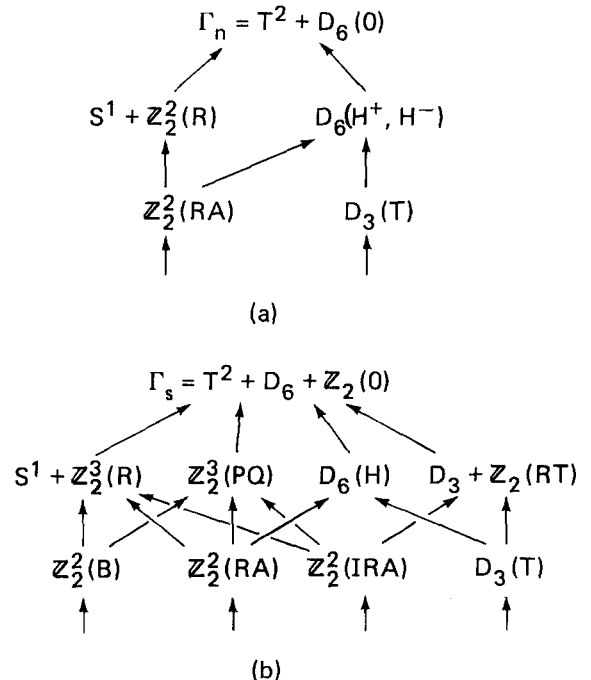


Fig. 3. Lattice of isotropy subgroups for the group (a) Γ_n (the nonsymmetric case) and (b) Γ_s (the symmetric case). Inclusion is indicated by arrow.

Γ_8 . In the former case the next most symmetric solutions have the (maximal) isotropy subgroups $S^1 + Z_2^2$ and D_6 , the former being the symmetry of rolls, the latter the symmetry of the hexagons (H^+ or H^-). In the figure inclusion is indicated by arrows. Observe that a single isotropy subgroup (e.g., D_6) may be the symmetry group for several different types of solutions (H^+, H^-). For the 12-dimensional representation corresponding to fig. 1d the lattices of isotropy subgroups are different. This is because the amplitude equations are now on C^6 rather than C^3 and the action of the group Γ_n is different. In fig. 3 we have also indicated the type of solution that is associated with each isotropy subgroup (cf. Tables I and II).

In describing the various solutions we use the

notation $z_\alpha = x_\alpha + iy_\alpha$. We list in table IA one representative of each orbit of the action of Γ_n on C^3 . In this way we enumerate all possible time-independent solutions to the amplitude equation (2.6) and (2.7). Which solutions actually occur depends on the specific invariant functions present in eqs. (2.6) and (2.7); these have to be computed from the Boussinesq equations (11). We also give the isotropy subgroups and the nomenclature, where relevant, for these solutions.

An important observation concerns the fixed point set F_z of the isotropy subgroup of a given point z . Let Σ_z be an isotropy subgroup and let

$$F_z = \{w \in C^3 | \gamma w = w \text{ for all } \gamma \in \Sigma_z\}. \tag{2.10}$$

Observe that if $g(z, \lambda)$ satisfies (2.3) then

Table IA
The non-symmetric case ($\Gamma = \Gamma_n$)

Nomenclature	Orbit representative	Isotropy subgroup
I. Trivial solution (O) (pure conduction)	$z = 0$	Γ_n
II. Rolls (R)	$x_1 > 0, y_1 = z_2 = z_3 = 0$	$S^1 + \{\sigma_v, c\}$
III. Hexagons (H)	$x_1 = x_2 = x_3 \neq 0$ $y_1 = y_2 = y_3 = 0$	$D_3 + \{c\}$
l-hexagons (H^+)	$x_1 > 0$	
g-hexagons (H^-)	$x_1 < 0$	
IV. Rectangles (RA)	$x_1 \neq x_2 = x_3 \neq 0$ $y_1 = y_2 = y_3 = 0$	$Z_2^2 = \{\sigma_v, c\}$
$A = x_1/ x_2 $		
RA ⁺ ($A > 0$)	$x_1 > 0$	
RA ⁻ ($A < 0$)	$x_1 < 0$	
Patchwork quilt (PQ) ($A = 0$)	$x_1 = 0$	
V. Triangles (T)	$z_1 = z_2 = z_3 = z \exp(i\Phi/3)$ $\text{Im}(z_1) \neq 0$ (i.e., $\Phi \neq 0, \pi$)	D_3
Regular triangles (RT)	$\text{Re}(z_1) = 0$ ($\Phi = \pi/2, 3\pi/2$)	
VI.	$x_2 = x_3$ $u_1 \neq u_2$ $y_1 > 0, y_2 = y_3 = 0$	$Z_2 = \{\sigma_v\}$
VII.	$y_1 = y_2 = y_3 = 0$ $u_2 < u_1 < u_3$	$Z_2 = \{c\}$
VIII.	$y_1 = y_3 = 0$ $u_2 < u_1 < u_3, y_2 > 0$	$\{1\}$

where $S^1: z \mapsto (z_1, e^{-i\theta}z_2, e^{i\theta}z_3)$
 $D_3: \text{permutation group of } z_1, z_2, z_3$
 $\sigma_v: z \mapsto (z_1, z_3, z_2)$
 $c: z \mapsto \bar{z}$

Table 1B
The non-symmetric case ($\Gamma = \Gamma_n$)

Σ_z	F_z	$\dim F_z$	$g F_z \times \mathbb{R} = 0$
II. $S^1 + \{\sigma_v, c\}$	$\mathbb{R}\{(1, 0, 0)\}$	1	$h_1 + x_1^2 h_3 + x_1^4 h_5 = 0$ $\sigma_1 = x_1^2, \sigma_2 = \sigma_3 = q = 0$
III. $D_3 + \{c\}$	$\mathbb{R}\{(1, 1, 1)\}$	1	$h_1 + x_1^2 h_3 + x_1^4 h_5$ $+ x_1(p_2 + x_1^2 p_4 + x_1^4 p_6) = 0$ $\sigma_1 = 3x_1^2, \sigma_2 = 3x_1^4, \sigma_3 = x_1^6, \sigma_4 = 2x_1^3$
IV. $\{\sigma_v, c\}$	$\mathbb{R}\{(1, 0, 0), (0, 1, 1)\}$	2	$h_1 + x_1^2 h_3 + x_1^4 h_5$ $+ x_1(p_2 + x_1^2 p_4 + y_1^2 p_6) = 0$ $x_1[h_3 + (x_1^2 + x_2^2)h_5 + x_1 x_2^2 p_6] = p_2$ $q = 2x_1 x_2^2$
V. D_3	$C\{(1, 1, 1)\}$	2	$h_1 + u_1 h_3 + u_1^2 h_5 = 0$ $p_2 + u_1 p_4 + u_1^2 p_6 = 0$
VI. Z_2	$\mathbb{R}\{(0, 1, 1), (1, 0, 0), (i, 0, 0)\}$	3	$h_1 + u_2 h_3 + u_2^2 h_5 = 0$ $p_2 + u_2 p_4 + u_2^2 p_6 = 0$ $h_3 + (u_1 + u_2)h_5 = 0$ $p_4 + (u_1 + u_2)p_6 = 0$
VII. $\{c\}$	$\mathbb{R}\{(1, 0, 0), (0, 1, 0), (0, 0, 1)\}$	3	$x_j(h_1 + u_j h_3 + u_j^2 h_5)$ $+ x_\alpha x_\beta (p_2 + u_j p_4 + u_j^2 p_6) = 0$ $j = 1, 2, 3.$ $\alpha, \beta = \text{indices not equal to } j$
VIII. $\{1\}$	C^3	6	$h_1 = h_3 = h_5 = 0$ $p_2 = p_4 = p_6 = 0$

Table IIA
The symmetric case ($\Gamma = \Gamma_s$)

	Nomenclature	Orbit representative	Isotropy subgroup
I.	Trivial solution (0) (pure conduction)	$z = 0$	Γ_s
II.	Rolls (R)	$x_1 > 0, y_1 = 0, z_2 = z_3 = 0$	$S^1 + \{\sigma_v, c, F_3\}$
III.	Hexagons (H)	$x_1 = x_2 = x_3 > 0$ $y_1 = y_2 = y_3 = 0$	$D_3 + \{c\}$
IV.	Patchwork quilt (PQ)	$x_2 = x_3 > 0$ $z_1 = y_2 = y_3 = 0$	$\{\sigma_v, c, F_1\}$
V.	Regular triangles (RT)	$y_1 = y_2 = y_3 > 0$ $x_1 = x_2 = x_3 = 0$	$D_3 + \{\bar{\sigma}_h\}$
VI.	Triangles (T)	$x_1 = x_2 = x_3 > 0$ $y_1 = y_2 = y_3 > 0$	D_3
VII.	Rectangles (RA)	$0 \neq x_1 \neq x_2 = x_3 > 0$ $y_1 = y_2 = y_3 = 0$	$Z_2^2 = \{\sigma_v, c\}$
VIII.	Imaginary rectangles (IRA)	$x_1 = x_2 = x_3 = 0$ $0 \neq y_1 \neq y_2 = y_3 > 0$	$Z_2^2 = \{\sigma_v, \bar{\sigma}_h\}$
IX.	Bimodal (B)	$x_1 > x_2 > x_3 = 0$ $y_1 = y_2 = y_3 = 0$	$Z_2^2 = \{F_3, C\}$

where S^1, D_3, σ_v and c are given in table I and

- $\bar{\sigma}_h: z \mapsto -\bar{z}$
- $F_1: z \mapsto (-z_1, z_2, z_3)$
- $F_3: z \mapsto (z_1, z_2, -z_3)$

Table IIB
The symmetric case ($\Gamma = \Gamma_3$)

Σ_z	F_z	$\dim F_z$	$g _{F_z \times \mathbf{R} = 0}$
II. $S^1 + \{\sigma_v, c, F_3\}$	$\mathbf{R}\{(1, 0, 0)\}$	1	$l_1 + x_1^2 l_3 + x_1^4 l_5 = 0$ $\sigma_1 = x_1^2, \sigma_2 = \sigma_3 = q = 0$
III. $D_3 + \{c\}$	$\mathbf{R}\{(1, 1, 1)\}$	1	$l_1 + x_1^2 l_3 + x_1^4 l_5$ $+ 2x_1^4(m_5 + x_1^2 m_7 + x_1^4 m_9) = 0$ $\sigma_1 = 3x_1^2, \sigma_2 = 3x_1^4, \sigma_3 = x_1^6, q = 2x_1^3$
IV. $\{\sigma_v, c, F_1\}$	$\mathbf{R}\{(0, 1, 1)\}$	1	$l_1 + x_2^2 l_3 + x_2^4 l_5 = 0$ $\sigma_1 = 2x_2^2, \sigma_2 = x_2^4, \sigma_3 = q = 0$
V. $D_3 + \{\bar{\sigma}_h\}$	$\mathbf{R}\{(i, i, i)\}$	1	$l_1 + y_1^2 l_3 + y_1^4 l_5 = 0$ $\sigma_1 = 3y_1^2, \sigma_2 = 3y_1^4, \sigma_3 = y_1^6, q = 0$
VI. D_3	$\mathbf{C}\{(1, 1, 1)\}$	2	$l_1 + u_1 l_3 + u_1^2 l_5 = 0$ $m_5 + u_1 m_7 + u_1^2 m_9 = 0$ $\sigma_1 = 3u_1, \sigma_2 = 3u_1^2$ $\sigma_3 = u_1^3, q \neq 0$
VII. $\{\sigma_v, c\}$	$\mathbf{R}\{(1, 0, 0), (0, 1, 1)\}$	2	$l_1 + x_1^2 l_3 + x_1^4 l_5$ $+ x_2^4(m_5 + x_1^2 m_7 + x_1^4 m_9) = 0$ $l_1 + x_2^2 l_3 + x_2^4 l_5$ $+ x_1^2 x_2^2(m_5 + x_2^2 m_7 + x_2^4 m_9) = 0$ $\sigma_1 = x_1^2 + 2x_2^2, \sigma_2 = 2x_1^2 x_2^2 + x_2^4$ $\sigma_3 = x_1^2 x_2^4, q = 2x_1 x_2^2$
VIII. $\{\sigma_v, \bar{\sigma}_h\}$	$\mathbf{R}\{(i, 0, 0), (0, i, i)\}$	2	$l_1 + y_1^2 l_3 + y_1^4 l_5 = 0$ $l_3 + l_5(y_1^2 + y_2^2) = 0$ $\sigma_1 = y_1^2 + 2y_2^2, \sigma_2 = 2y_1^2 y_2^2 + y_2^4$ $\sigma_3 = y_1^2 y_2^4, q = 0$
IX. $\{c, F_3\}$	$\mathbf{R}\{(1, 0, 0), (0, 1, 0)\}$	2	$l_1 + x_1^2 l_3 + x_1^4 l_5 = 0$ $l_3 + l_5(x_1^2 + x_2^2) = 0$ $\sigma_1 = x_1^2 + x_2^2, \sigma_2 = x_1^2 x_2^2, \sigma_3 = q = 0$

$g: F_z \times \mathbf{R} \rightarrow F_z$. For if $\gamma w = w$ then $g(w, \lambda) = g(\gamma w, \lambda) = \gamma g(w, \lambda)$. Thus, $g(w, \lambda) \in F_z$ if $w \in F_z$. It follows that if one looks for solutions with a given isotropy subgroup Σ_z one need only solve $g|_{F_z \times \mathbf{R}} = 0$ to find such solutions. For example, for rolls one sees that $F_z = \mathbf{R}\{1, 0, 0\}$ is one-dimensional and $g|_{F_z \times \mathbf{R}} = (l_1 x + l_3 x^3 + l_5 x^5, 0, 0)$ where $l_j = l_j(x_1^2, 0, 0, 0, \lambda)$. One then sees that non-trivial roll solutions are defined by $l_1 + l_3 x_1^2 + l_5 x_1^4 = 0$. In table IB we list each of the solution types along with the fixed point sets F_z and the explicit equations of $g|_{F_z \times \mathbf{R}} = 0$. Note that each of the maximal isotropy subgroups have one-dimensional fixed point sets.

Both the triangles and the rectangles have two-dimensional fixed point sets. This means that the

amplitude alone does not determine the solution.

The triangles are equal amplitude solutions: $u_1 = u_2 = u_3$. They are conveniently parametrized by the amplitude and the sum of the phases, Φ . That is, let $z_\alpha = \sqrt{u_\alpha} e^{i\phi_\alpha}$ and let

$$\Phi = \phi_1 + \phi_2 + \phi_3 \pmod{2\pi}. \tag{2.11}$$

In this notation l -hexagons (H^+) have $\Phi = 0$, g -hexagons (H^-) have $\Phi = \pi$, and regular triangles have $\Phi = \pi/2$ or $3\pi/2$. A translation of the origin $x \rightarrow x + d$, in eq. (2.1) changes $z_\alpha \rightarrow z_\alpha e^{ik_\alpha \cdot d}$; therefore Φ is an invariant of translations. Complex conjugation, however, changes the sign of Φ ; $c(\Phi) = -\Phi$ and the horizontal reflection changes Φ as follows:

$$\sigma_h(\phi_\alpha) = \pi - \phi_\alpha \quad \text{and} \quad \sigma_h(\Phi) = \pi - \Phi.$$

We can therefore choose Φ in the interval

$$\Phi \in [0, \pi] \quad \text{for } \Gamma_n,$$

$$\Phi \in \left[0, \frac{\pi}{2}\right], \quad \text{for } \Gamma_s,$$

In addition, of course, Φ is only defined if all of the amplitudes are nonzero.

The rectangles have two equal amplitudes, and one different. In addition, they are real solutions, i.e., $\Phi = O(RA^+)$, or $\pi(RA^-)$. They are conveniently parametrized by the ratio of the two amplitudes, A (cf. table IA).

The triangle and rectangle solutions have a rich structure. They are visualized here in two ways, both looking from above. In figs. 4 and 5 we shade the “hot” regions, where $\theta(x, y) > 0$ (cf. eq. (2.1)). Note that this is also where the vertical velocity w is upwards. These figures also indicate the unit hexagonal cell. In figs. 4a and 4b we draw the horizontal velocity field (u, v) in a horizontal plane $y = y_0 > 0$. Note that this is proportional to $\nabla_x \theta(x, y_0)$. For free-free boundaries this is the form of the streamlines at the upper plate. In the streamline pictures the unit cell is chosen in such a way that the boundary is a streamline. In each case, the plane can be tiled with the unit cell shown.

For the rectangles the two visualizations emphasize different singular solutions. For $|A| < 2$ the hot regions are disconnected (these are the false hexagons of Buzano and Golubitsky). For $|A| > 2$ the hot regions in neighboring hexagons become connected (these are the wavy rolls). Fig. 4b emphasizes this transition by showing the cases $A = 3/2, 2, 5/2$. As $A \rightarrow \infty$ the rectangles approach the rolls.

Fig. 4a shows that a fixed point of the flow undergoes a pitchfork bifurcation to three fixed points at $A = 1/2$. This is illustrated by showing the horizontal flow lines for $A = 1/4, 1/2, 3/4$. Note finally that the rectangle with $A = \pm 1$ is a hexagon H^\pm , and the triangle with $\Phi = 0$ or π is also a hexagon H^\pm .

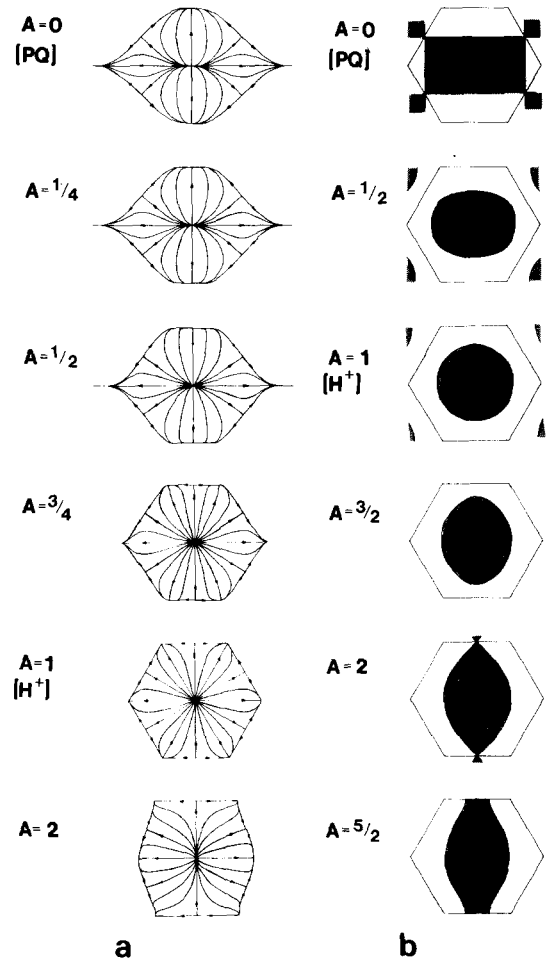


Fig. 4. Rectangles (RA) for different values of the amplitude ratio A . The solutions are visualized using the temperature variation on a horizontal plane $\theta(x) = A \cos k_1 \cdot x + \cos k_2 \cdot x + \cos k_3 \cdot x$: (a) streamlines of the horizontal velocity field $(u, v) = \nabla_x \theta$; (b) hot rising regions $\theta > 0$ (shaded), cold descending regions $\theta < 0$ (unshaded). At $A = \frac{1}{2}$ the local minimum of θ at $x = (0, 2\pi/\sqrt{3})$ changes to a saddle point via a pitchfork bifurcation (fig. a). Fig. (b) shows the transition (at $|A| = 2$) from “false hexagons” with disconnected rising regions to “wavy rolls” in which the rising regions are connected.

For both triangles and rectangles there is a single exceptional solution that has an additional mid-plane reflection symmetry: the patchwork quilt ($A = 0$) and the regular triangle ($\Phi = \pi/2$). Both solutions have a symmetry between hot and cold, as seen in figs. 4 and 5. These solutions are of interest for the problem with the Γ_s symmetry. The isotropy group of regular triangles in Γ_s includes the mid-

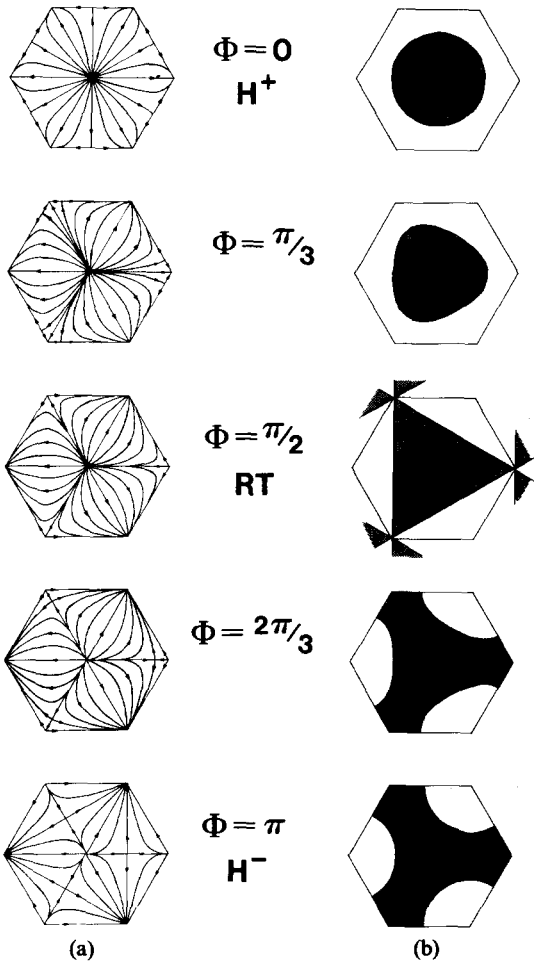


Fig. 5. Triangles (T) for different values of the sum of the phases, Φ . The visualization is the same as in fig. 4, but with $\theta(x) = \cos(k_1 \cdot x + \Phi/3) + \cos(k_2 \cdot x + \Phi/3) + \cos(k_3 \cdot x + \Phi/3)$.

plane reflection, which interchanges hot and cold, coupled with a 180° rotation (i.e., $\bar{\sigma}_h: z \mapsto -\bar{z}$). The isotropy group of the patchwork quilt in Γ_s includes the midplane reflection coupled with a translation (i.e., $F_1: z \mapsto -(z_1, e^{-in_2 z_2}, e^{in_3 z_3})$). Moreover, the isotropy subgroups of the patchwork quilt and regular triangles are maximal isotropy subgroups of Γ_s (cf. fig. 3). Note, finally, that the roll also has an additional symmetry in the group Γ_s .

We present in table IIA orbit representatives for each of the maximal isotropy subgroups of Γ_s . In table IIB we give the fixed point sets, F_z , and

$g|_{F_z \times \mathbb{R}}$, where g is assumed to have the form given in eq. (2.7). Note that H^+ and H^- hexagons are identified by the midplane reflection.

3. The bifurcation diagrams for the symmetric case

In this section we describe the computation of the possible bifurcation diagrams describing the onset of convection in a system with midplane reflection symmetry. The calculation proceeds in three stages. First, the possible steady state solutions of the amplitude equations (2.7) are determined. Then, their linearized (orbital) stability is calculated, followed by the construction of the bifurcation diagrams. The bifurcation diagrams describe the variation in the number and stability of the steady solutions as the bifurcation parameter λ is varied. The results of this section follow from the assumption that $g(z, \lambda)$ commutes with the symmetry group Γ_s , i.e., that it has the form (2.7). The corresponding results for the non-symmetric case are given by Buzano and Golubitsky [1].

3.1. The solution branches

The number and nature of the steady state solutions of $g(z, \lambda) = 0$ is described by the following result:

Theorem 1. Assume that $\dot{z} = g(z, \lambda)$ is of the form (2.7) with

$$\begin{aligned}
 l_1(0) &= 0, & l_{1,\lambda}(0) &\neq 0, & l_{1,\sigma_1}(0) + l_3(0) &\neq 0, \\
 2l_{1,\sigma_1}(0) + l_3(0) &\neq 0, \\
 3l_{1,\sigma_1}(0) + l_3(0) &\neq 0, & l_3(0) &\neq 0, & m_5(0) &\neq 0.
 \end{aligned}
 \tag{3.1}$$

Then there are precisely four non-trivial branches of solutions to $g(z, \lambda) = 0$ in the neighborhood of $(z, \lambda) = 0$ corresponding one each to rolls, hexagons, regular triangles, and the patchwork quilt. These branches are supercritical if:

Rolls

$$(l_{1,\sigma_1}(0) + l_3(0))l_{1,\lambda}(0) < 0,$$

Hexagons

Regular triangles

$$(3l_{1,\sigma_1}(0) + l_3(0))l_{1,\lambda}(0) < 0,$$

Patchwork quilt

$$(2l_{1,\sigma_1}(0) + l_3(0))l_{1,\lambda}(0) < 0.$$

If any of these inequalities are reversed, the corresponding branch is subcritical.

Remark. The equality $l_1(0) = 0$ is called a *defining condition*; it is the statement that $z = 0, \lambda = 0$ is a bifurcation point. The inequalities are called *non-degeneracy conditions*, since they are satisfied generically. We are therefore describing the least degenerate bifurcation consistent with the Γ_5 symmetry.

Proof. The proof of the existence of these four branches is straightforward. Consider, in table IIB, the calculation of $\tilde{g} = g|_{F_2 \times \mathbb{R}}$ and write out the lowest order terms in the Taylor expansion of \tilde{g} . If these lowest order terms are nonzero, then one proves the existence of the branches using the implicit function theorem. The calculations yield

Rolls:

$$\lambda = -\frac{l_{1,\sigma_1}(0) + l_3(0)}{l_{1,\lambda}(0)}\sigma_1 + \dots,$$

Hexagons:

$$\lambda = -\frac{3l_{1,\sigma_1}(0) + l_3(0)}{l_{1,\lambda}(0)}\frac{\sigma_1}{3} + \dots,$$

Regular triangles:

$$\lambda = -\frac{3l_{1,\sigma_1}(0) + l_3(0)}{l_{1,\lambda}(0)}\frac{\sigma_1}{3} + \dots,$$

Patchwork quilt:

$$\lambda = -\frac{2l_{1,\sigma_1}(0) + l_3(0)}{l_{1,\lambda}(0)}\frac{\sigma_1}{2} + \dots$$

These results show that for each of the above solution types the amplitude is specified uniquely for each λ .

To show that there are no solutions near the origin other than the four listed in theorem 1, consider the 3 cases:

- (1) $u_1 \neq 0, u_2 = u_3 = 0$;
- (2) $u_1 \neq 0, u_2 \neq 0, u_3 = 0$;
- (3) $u_1 \neq 0, u_2 \neq 0, u_3 \neq 0$.

There is only one type of solution in case (1), the rolls. For case (2), first note that $q = 0$. Therefore

$$\begin{aligned} \dot{z}_1 &= z_1(l_1 + u_1l_3 + u_1^2l_5) = 0, \\ \dot{z}_2 &= z_2(l_1 + u_2l_3 + u_2^2l_5) = 0, \\ \dot{z}_3 &= 0. \end{aligned}$$

Since $z_1 \neq 0, z_2 \neq 0$ we know

$$l_1 + u_1l_3 + u_1^2l_5 = l_1 + u_2l_3 + u_2^2l_5 = 0.$$

Therefore

$$(u_1 - u_2)[l_3 + (u_1 + u_2)l_5] = 0.$$

So either

$$u_1 = u_2 \quad \text{or} \quad l_3 + \mathcal{O}(z^2) = 0.$$

Since $l_3(0) \neq 0$ the only solution near the origin is $u_1 = u_2$ (the patchwork quilt).

For case (3), we will first show that the 3 amplitudes must be equal, then we will show that only hexagons and regular triangles are found near the origin. Observe that

$$\begin{aligned} 0 &= z_2\dot{z}_1 - z_1\dot{z}_2 = z_1z_2(u_1 - u_2) \\ &\quad \times \left[l_3 + (u_1 + u_2)l_5 - \frac{\bar{z}_3 q}{z_1z_2}m_5 + \mathcal{O}(z^4) \right]. \end{aligned} \quad (3.2)$$

By assumption $z_1 z_2 \neq 0$, and $l_3(0) \neq 0$ so the only small amplitude solutions have $u_1 = u_2$. Similarly, we find that $u_1 = u_2 = u_3$.

Since all amplitudes are nonzero, the phases ϕ_α are all defined, and we can write

$$\begin{aligned} \dot{\phi}_1 &= \frac{(\bar{z}_1 \dot{z}_1 - z_1 \dot{\bar{z}}_1)}{2iu_1} \\ &= -2u_2 u_3 \cos \Phi \sin \Phi (m_5 + u_1 m_7 + u_1^2 m_9) = 0. \end{aligned} \tag{3.3}$$

Since $m_5(0) \neq 0$, we must have $\cos \Phi \sin \Phi = 0$, or $\Phi = n\pi/2$. These are the hexagons and regular triangles.

Note that if the amplitude equations are truncated at third order, then Triangles of all phases are solutions in the symmetric case. Therefore, one must consider the 5th order term $m_5(0)$ when classifying these solutions. This term has been neglected in the past because the rolls are stable in the symmetric Rayleigh–Bénard convection. It seems likely, however, that other physical systems with the Γ_s symmetry, in convection or elsewhere, may have stable hexagons or triangles.

It is appropriate to remark here that it is generally true that there exist solution branches corresponding to isotropy subgroups Σ_z whose fixed point set F_z is one-dimensional. Such isotropy subgroups have to be maximal in the lattice of isotropy subgroups. This observation follows from a result of L. Michel. (See Golubitsky [10]). Thus, in our case, the existence of at least four solution branches is guaranteed by general considerations.

3.2. Linearized orbital stability

As we noted in section 1, when a mapping g commutes with a group Γ , if g vanishes at a point, then it does so on its entire orbit. If the dimension of the orbit is a positive integer s then the Jacobian of g , dg , is forced to have s eigenvalues equal to zero. The null eigenvectors correspond to spatial translations of the pattern. It is impossible for such solutions to be linearly stable. What is possible is that every eigenvalue of $(dg)_{z,\lambda}$ which is not con-

strained by the group action to be zero lies in the correct half plane for stability. A solution z, λ satisfying this last condition is called *linearly orbitally stable*-this is analogous to Poincaré's notion of *relative stability* for periodic orbits in Celestial mechanics that arise from a symmetry. Such solutions satisfy the following form of asymptotic stability. All \bar{z} sufficiently close to z tend exponentially in time to some point on the orbit $\Gamma \cdot z$ near z . Note that the four solution branches discussed above have orbits of positive dimension: 1 for rolls and 2 for hexagons, regular triangles and patchwork quilt. It follows that dg has one zero eigenvalue along the roll solutions and two zero eigenvalues along the other nontrivial branches of solutions.

The fact that $g(\gamma z, \lambda) = \gamma g(z, \lambda)$ for all $\gamma \in \Gamma$ gives another restriction on the Jacobian dg . In particular, the chain rule implies

$$(dg)_{\gamma z, \lambda} \gamma = \gamma (dg)_{z, \lambda}.$$

Thus, if γ is in the isotropy subgroup Σ_z ,

$$(dg)_{z, \lambda} \gamma = \gamma (dg)_{z, \lambda}. \tag{3.4}$$

For solutions with maximal isotropy subgroups in Γ_s the commutativity restriction (3.4) allows one to compute directly the eigenvalues of the 6×6 matrix $(dg)_{z, \lambda}$. These results are summarized in table IIIA. We assume that g commutes with Γ_s and has the form (2.7). We choose the ordering of the real coordinates on \mathbb{R}^6 to be $(x_1, x_2, x_3, y_1, y_2, y_3)$, first the real parts of z_1, z_2, z_3 and then the imaginary parts. In coordinates, g has the form

$$g(z, \lambda) = (g_1(z, \lambda), g_2(z, \lambda), \dots, g_6(z, \lambda)),$$

where

$$\begin{aligned} g_\alpha(z, \lambda) &= (l_1 + u_\alpha l_3 + u_\alpha^2 l_5) x_\alpha \\ &\quad + (m_5 + u_\alpha m_7 + u_\alpha^2 m_9) q \operatorname{Re}(\bar{z}_\beta \bar{z}_\gamma), \end{aligned} \tag{3.5a}$$

$$\begin{aligned} g_{\alpha+3}(z, \lambda) &= (l_1 + u_\alpha l_3 + u_\alpha^2 l_5) y_\alpha \\ &\quad + (m_5 + u_\alpha m_7 + u_\alpha^2 m_9) q \operatorname{Im}(\bar{z}_\beta \bar{z}_\gamma), \end{aligned} \tag{3.5b}$$

Table IIIA
The eigenvalues

I.	(O) $l_1(0, 0, 0, 0, \lambda)$ (six times)
II.	(R) A, D (four times), 0 where $A = x_1 \frac{\partial}{\partial x_1} (l_1 + x_1^2 l_3 + x_1^4 l_4)$ and $D = -x_1^2 l_3 - x_1^4 l_5$.
III.	(H) $A - B$ (twice), $A + 2B, 3\alpha, 0$ (twice) where $A = \frac{\partial g_1}{\partial x_1}, B = \frac{\partial g_1}{\partial x_2}$, and $\alpha = \frac{\partial g_4}{\partial y_1} = -2x_1^4(m_5 + x_1^2 m_7 + x_1^4 m_9)$.
IV.	(PQ) $A - B, A + B, E, \epsilon, 0$ (twice) where $A = \frac{\partial g_2}{\partial x_2}, B = \frac{\partial g_2}{\partial x_3}, E = \frac{\partial g_1}{\partial x_1}$, and $\epsilon = l_1$.
V.	(RT) $3A, C - D$ (twice), $C + 2D, 0$ (twice) where $A = \frac{\partial g_1}{\partial x_1} = 2y^4(m_5 + y^2 m_7 + y^4 m_9), C = \frac{\partial g_4}{\partial y_1}$, and $D = \frac{\partial g_4}{\partial y_2}$.

All eigenvalues in this table are real.

Table IIIB
The signs of the eigenvalues of $(dg)_{z,\lambda}$

I.	(O) $\text{sgn}(l_{1,\lambda}(0)\lambda)$ (six times)
II.	(R) $\text{sgn}(l_{1,\sigma_1}(0) + l_3(0)), -\text{sgn}(l_3(0))$ (four times), 0
III.	(H) $\text{sgn}(l_3(0))$ (twice), $\text{sgn}(3l_{1,\sigma_1}(0) + l_3(0)), -\text{sgn}(m_5(0)), 0$ (twice)
IV.	(PQ) $-\text{sgn}(l_3(0))$ (twice), $\text{sgn}(l_3(0)), \text{sgn}(2l_{1,\sigma_1}(0) + l_3(0)), 0$ (twice)
V.	(RT) $\text{sgn}(m_5(0)), \text{sgn}(l_3(0))$ (twice), $\text{sgn}(3l_{1,\sigma_1}(0) + l_3(0)), 0$ (twice)

and $\alpha = 1, 2, 3; \beta, \gamma$ are the integers in $\{1, 2, 3\}$ not equal to α .

The entries in table IIIA are obtained using elementary calculations based on these two restrictions. We shall describe here the calculations for the regular triangle solutions. The calculations for the other solution types are (mostly) given in Buzano and Golubitsky [1], theorem 5.5.

Let $L = (dg)_{z,\lambda}$ where $z = y(i, i, i)$ is a typical regular triangle with isotropy subgroup $D_3 + \{\bar{\sigma}_h\}$. Let L have the block diagonal form

$$L = \begin{pmatrix} P & Q \\ R & S \end{pmatrix},$$

where P, Q, R and S are 3×3 matrices. Observe that, $\bar{\sigma}_h$ has the matrix form

$$Q_1 = \begin{pmatrix} -I_3 & 0 \\ 0 & I_3 \end{pmatrix},$$

where I_3 is the 3×3 identity matrix. Restriction (3.4) states that L and Q_1 commute which implies that $Q = R = 0$. We also know that L must commute with D_3 . Since D_3 is just the permutation group on z_1, z_2, z_3 , this means that both P and S must commute with

$$Q_2 = \begin{pmatrix} 0 & 1 & 0 \\ 0 & 0 & 1 \\ 1 & 0 & 0 \end{pmatrix} \quad \text{and} \quad Q_3 = \begin{pmatrix} 0 & 1 & 0 \\ 1 & 0 & 0 \\ 0 & 0 & 1 \end{pmatrix}.$$

Thus

$$P = \begin{pmatrix} A & B & B \\ B & A & B \\ B & B & A \end{pmatrix} \quad \text{and} \quad S = \begin{pmatrix} C & D & D \\ D & C & D \\ D & D & C \end{pmatrix}.$$

To find the eigenvectors of L with zero eigenvalue which are forced by the group action, consider the curve

$$s \mapsto y(e^{is}, e^{-is}, i), \quad y \neq 0. \tag{3.6}$$

This curve is obtained by the action of $S^1 = (s, 0)$ inside the torus acting on $z = y(i, i, i)$. Differentiating (3.6) with respect to s and evaluating at $s = 0$ yields the desired eigenvector of L . One obtains $y(-1, 1, 0)$ in \mathbb{C}^3 or $y(-1, 1, 0, 0, 0, 0)$ in the real coordinates on \mathbb{R}^6 . It follows that $A = B$ in P .

The eigenvalues of L are just the eigenvalues of P and S . P is a rank one matrix with trace $3A$; its eigenvalues are $3A$ and 0 (twice). The eigenvalues of S are $C + 2D$ and $C - D$ (twice). To prove this, observe $(1, 1, 1)$, $(1, -1, 0)$ and $(0, 1, -1)$ are eigenvectors of S .

Now observe from the positions of A , C and D in L that $A = \partial g_1 / \partial x_1$, $C = \partial g_4 / \partial y_1$ and $D = \partial g_4 / \partial y_2$. Write

$$g_1 = Lx_1 + Mq \operatorname{Re}(\bar{z}_2 \bar{z}_3),$$

where

$$L = l_1 + u_1 l_3 + u_1^2 l_5 \quad \text{and} \quad M = m_5 + u_1 m_7 + u_1^2 m_9. \tag{3.7}$$

Recall from table IIB that $x_1 = 0$, $L = 0$ and $q = 0$ for regular triangles. It follows that for such solutions

$$\frac{\partial}{\partial x_1} g_1 = M \frac{\partial}{\partial x_1} q \operatorname{Re}(\bar{z}_2 \bar{z}_3) = 2y^4(m_5 + y^2 m_7 + y^4 m_9)$$

assuming that $z = y(i, i, i)$.

We can now state the main result of the section.

Theorem 2. Assume that $g(z, \lambda)$ commutes with Γ_s and satisfies the non-degeneracy conditions (3.1). Then the signs of the eigenvalues of $(dg)_{z,\lambda}$ are given in table IIIB.

Proof. To prove this theorem one simply computes the first non-zero term in the Taylor expansion of each eigenvalue given in table IIIA. Since the calculations are all similar, we give only those for the regular triangle solutions.

The sign of A in table IIIA (RT) is easily seen to be $\operatorname{sgn}(m_5(0))$ as long as $m_5(0) \neq 0$, which is assumed in (3.1). Using the notation of (3.7) observe that

$$g_4 = Ly_1 + Mq \operatorname{Im}(\bar{z}_2 \bar{z}_3).$$

Since L , q and $\operatorname{Im}(\bar{z}_2 \bar{z}_3)$ vanish at points $y(i, i, i)$ it follows that

$$C = \frac{\partial}{\partial y_1} g_4 = y \frac{\partial}{\partial y_1} L \quad \text{and} \quad D = \frac{\partial}{\partial y_2} g_4 = y \frac{\partial}{\partial y_2} L$$

at $z = y(i, i, i)$. Computing modulo terms of order y^3 one finds

$$C = 2(l_{1,\sigma_1}(0) + l_3(0))y^2 + \dots, \\ D = 2l_{1,\sigma_1}(0)y^2 + \dots$$

Note that we showed in theorem 1 that

$$\lambda = - \frac{3l_{1,\sigma_1}(0) + l_3(0)}{l_{1,\lambda}(0)} y^2 + \dots,$$

so that terms involving λ 's are higher order terms. It follows that

$$\operatorname{sgn}(C - D) = \operatorname{sgn} l_3(0)$$

and

$$\operatorname{sgn}(C + 2D) = \operatorname{sgn}(3l_{1,\sigma_1}(0) + l_3(0))$$

assuming that $l_3(0) \neq 0$ and $3l_{1,\sigma_1}(0) + l_3(0) \neq 0$. This calculation verifies tables IIIB, V.

3.3. The bifurcation diagrams

The description of the bifurcation diagrams associated with the Γ_s symmetry can be simplified by an appropriate scaling of the equations. Assume,

as in theorem 1, that $l_3(0) \neq 0$, $l_{1,\lambda}(0) \neq 0$ and $m_5(0) \neq 0$. Then we can make the following change of variables:

$$z \mapsto \alpha z, \quad t \mapsto t/\beta, \quad \lambda \mapsto \gamma \lambda, \tag{3.8}$$

where

$$\begin{aligned} \alpha^2 &= |l_3(0)/m_5(0)|, \quad \beta = |l_3(0)/m_5(0)|l_3(0), \\ \gamma &= -|l_3(0)/m_5(0)|l_3(0)/l_{1,\lambda}(0). \end{aligned} \tag{3.9}$$

In terms of the new variables the amplitude equations (2.7) are

$$\dot{z}_1 = z_1(-\lambda + a\sigma_1 + u_1) + cq\bar{z}_2\bar{z}_3 + \mathcal{O}(z^5, \lambda^2z, \lambda z^2), \tag{3.10}$$

where

$$a = l_{1,\sigma_1}(0)/l_3(0), \quad c = \text{sgn}(m_5(0)l_3(0)). \tag{3.11}$$

Note that the nondegeneracy conditions (3.1) imply that

$$a \neq -1, \quad a \neq -\frac{1}{2}, \quad c = \pm 1. \tag{3.12}$$

The additional nondegeneracy conditions are implicit in the form (3.10) of the amplitude equations.

In applications, it is important to notice that our scaling of the equations involves a time reversal if $\text{sgn}(l_3(0)) = -1$. This has the effect of reversing the stability assignments. Therefore, in our analysis of eq. (3.10), positive eigenvalues imply stability if $\text{sgn}(l_3(0)) = -1$. Similarly, the direction of increasing λ depends on $\text{sgn}(l_{1,\lambda}(0)l_3(0))$. If this quan-

tity is negative, the bifurcation diagrams (figs. 6–11) should be read with λ increasing from right to left.

The results of theorems 1 and 2 are summarized for the scaled equation in table IV. Note that we have omitted the zero eigenvalues forced by the symmetry of the pattern both in this table and in the bifurcation diagram. The bifurcation diagrams are amplitude-Rayleigh number diagrams. The amplitude is conveniently measured by σ_1 since the convective heat transport across the fluid layer is proportional to $\sigma_1 + \mathcal{O}(z^4)$. Thus, the bifurcation diagrams shown in figs. 6–11 are drawn in a form that can easily be compared to experiment.

The diagrams shown in fig. 6 are drawn as if the fifth order terms $z_1\sigma_1^2$, $z_1\sigma_1u_1$ and $z_1u_1^2$ in eq. (3.10) are zero. These terms do not affect the relative amplitudes of the branches or their stability properties. One such term does, however, enter in the singularity theory analysis of the problem (see section 4). In the diagrams the number of positive and negative eigenvalues is indicated on each branch. Note that the fifth order term c determines the sign of the eigenvalue associated with the phase Φ of the hexagons and regular triangles, since $\dot{\Phi} = -c\sigma_2\sin\Phi\cos\Phi$ (cf. eq. (3.3)), as well as their relative amplitudes.

For $a < -1$ and $l_3(0) > 0$, the rolls are supercritical and stable, as illustrated in fig. 6; note that $R - R_c$ is proportional to $-\lambda$. For ordinary Rayleigh-Bénard convection in a Boussinesq fluid with free-free or rigid-rigid perfectly conducting boundaries, Schlüter, Lortz and Busse [3] have shown that $a < -1$ for all Prandtl numbers. In

Table IV
Normalized bifurcation data

Solution branch	Eigenvalue (to lowest nontrivial order)
I. (0) $z = 0$	$-\lambda$ (6 times)
II. (R) $\lambda = (a + 1)\sigma_1 + \dots$	$-\sigma_1$ (4 times), $2(a + 1)\sigma_1$
III. (H) $\lambda = (a + \frac{1}{3})\sigma_1 + \dots$	$\frac{2}{3}\sigma_1$ (twice), $\frac{2}{3}(3a + 1)\sigma_1$, $-\frac{2}{3}c\sigma_1^2$
IV. (PQ) $\lambda = (a + \frac{1}{2})\sigma_1 + \dots$	σ_1 , $-\frac{1}{2}\sigma_1$, $-\frac{1}{2}\sigma_1$, $(2a + 1)\sigma_1$
V. (RT) $\lambda = (a + \frac{1}{3})\sigma_1 + \dots$	$\frac{2}{3}\sigma_1$ (twice), $\frac{2}{3}(3a + 1)\sigma_1$, $\frac{2}{3}c\sigma_1^2$

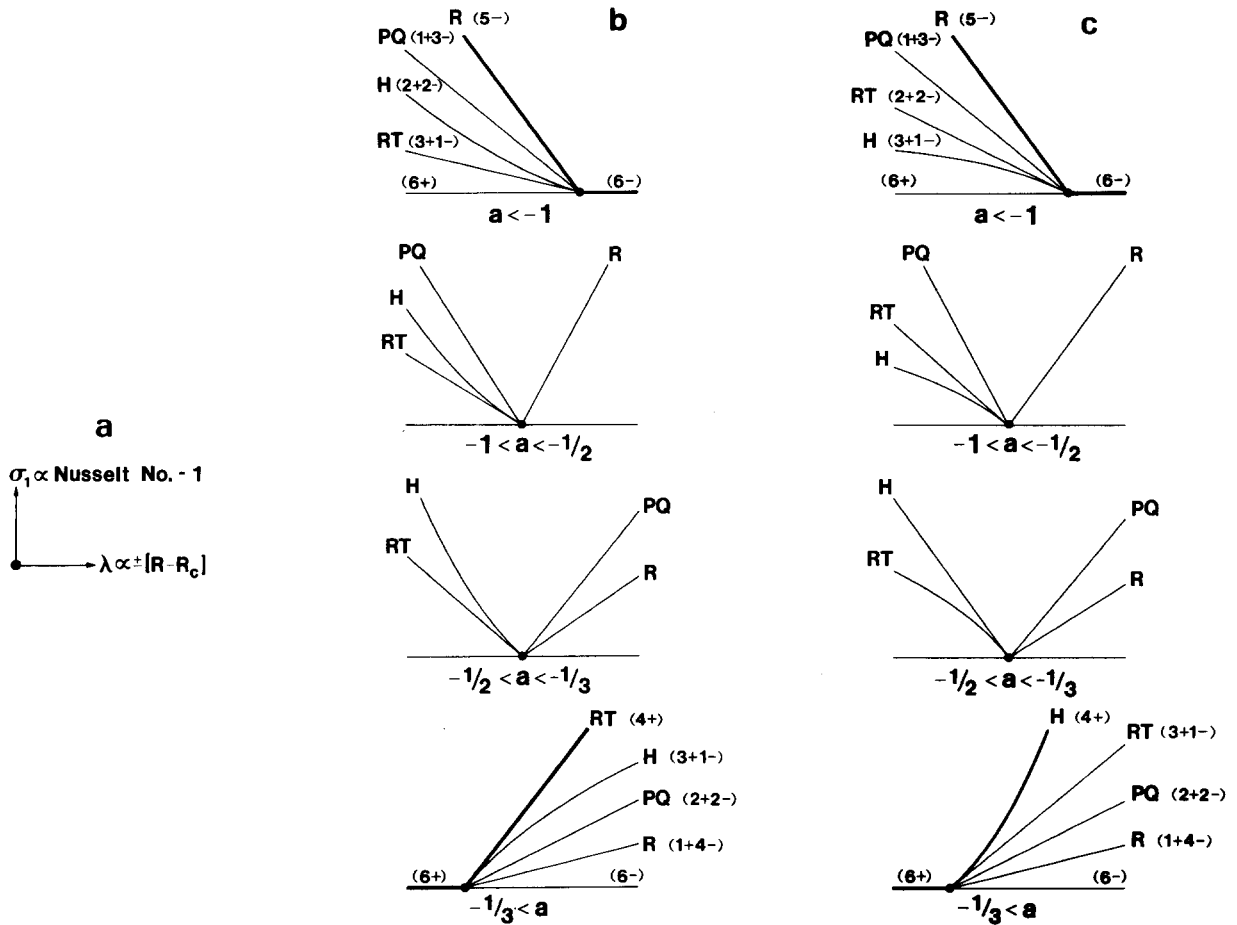


Fig. 6. The bifurcation diagrams in figs. 6–11 show the variation of the convective heat transport (σ_1) with the Rayleigh number ($\pm \lambda$), (fig. 6a). The bifurcation diagrams for the problem with midplane reflection symmetry as computed from eq. (3.10) are drawn for $c = 1$ (fig. 6b), and $c = -1$ (fig. 6c). The number of positive and negative eigenvalues is indicated, with zero eigenvalues omitted. Eigenvalues not shown are obtained from continuity. As the parameter a is increased, a single eigenvalue changes sign when a subcritical branch becomes supercritical. The eigenvalues of rolls (R) and the patchwork quilt (PQ) are the same for $c = \pm 1$. Possible stable solutions are indicated by heavy lines. Either positive or negative eigenvalues can be considered stable, depending on the direction of time.

these cases rolls occur near the onset of instability. For $a > -\frac{1}{3}$ and $l_3(0) > 0$, the hexagons are stable if $m_5(0) < 0$ and the regular triangles are stable if $m_5(0) > 0$. This possibility is of considerable interest, and we shall return to it in section 5. From a physical point of view the two diagrams in the region $-1 < a < -\frac{1}{3}$ are incomplete, since there is no stable solution near the origin. Of course, we expect some branch to turn over and become stable at large amplitude via a saddle-node bifurcation.

This, however, is not accessible to a small amplitude theory unless one studies a more degenerate bifurcation with, say, $a = -1$. The universal unfolding of such a degenerate bifurcation captures the secondary bifurcations. Such studies, however, require the full machinery of singularity theory, and we do not pursue them here. Note finally that if a stable solution exists, it is the one with the maximum heat transport.

This is often, but not always, the case (cf. fig. 9).

4. Comparison with the non-symmetric problem

The bifurcations off the conductive solution in the convection problem without midplane reflectional symmetry are described in detail by Buzano and Golubitsky (1). These results are quite different from those obtained in section 3 for the case with the reflectional symmetry. In this section we describe Buzano and Golubitsky's results and provide a connection with the results of section 3. It is important to establish such a connection in order to understand how the bifurcation diagrams presented in section 3 deform into those of Buzano and Golubitsky when the midplane reflectional symmetry is broken. The symmetry can be broken by making the linearized problem nonselfadjoint, or it can be broken at higher order in a problem that remains selfadjoint. We shall show that for those symmetric problems in which hexagons or regular triangles are stable, there are observable differences between the two possibilities.

The results of Buzano and Golubitsky are obtained by the methods of singularity theory. The methods of the present paper cannot provide an acceptable description of the bifurcation behavior in the non-symmetric problem because none of the bifurcation branches is stable at small amplitude. In order to capture aspects of large amplitude, it is necessary to consider a degenerate bifurcation for which the coefficient of the quadratic term in eq. (2.6) vanishes. By examining the bifurcation diagrams for small values of this coefficient, secondary bifurcations that enable some of the bifurcating solution branches to gain stability are brought to small amplitudes and appear in the local bifurcation diagrams. The analysis of degenerate bifurcations (i.e., bifurcations in which some of the nondegeneracy conditions are violated) requires the more sophisticated methods of singularity theory. In order to relate the results of the problem with the midplane reflection symmetry to those without, we must first restate our results in the context of singularity theory.

4.1. Singularity theory and normal forms

Both methods start with the amplitude equations (2.6) or (2.7). In the present paper, we were able to show that if certain nondegeneracy conditions hold then the bifurcation behavior near the origin $(z, \lambda) = 0$ is described completely by the leading terms in the Taylor expansion of the invariant functions l_i, m_i in the amplitude equations (2.7). In a sense to be explained the addition of the higher order terms to (3.10) does not effect the nature of the steady state solutions: the bifurcation diagrams are structurally stable.

Singularity theory studies solutions of the steady state equations

$$g(x, \lambda) = 0, \quad g: \mathbb{R}^n \times \mathbb{R} \rightarrow \mathbb{R}^n, \tag{4.1}$$

in the neighborhood of a *singularity* defined by

$$g(0, 0) = d_x g(0, 0) = 0. \tag{4.2}$$

These conditions define a bifurcation problem. Singularity theory seeks to simplify the form of g near the singularity $(0, 0)$, while preserving its zero set and symmetry properties, by means of independent coordinate changes in the range and domain:

$$h(x, \lambda) = S(x, \lambda)g(X(x, \lambda), \Lambda(\lambda)), \tag{4.3a}$$

where

$$\begin{aligned} \Lambda(0) = 0, \quad \Lambda'(0) = c_1, \quad X(0, 0) = 0, \\ d_x X(0, 0) = c_2 I, \quad S(0, 0) = c_3 I, \\ c_1 \neq 0, \quad c_2 \neq 0, \quad c_3 \neq 0, \end{aligned} \tag{4.3b}$$

and X and S commute with all elements γ of the symmetry group Γ of g . We shall call h and g related by (4.3) Γ -equivalent, and write $g \approx_{\Gamma} h$. The freedom in the transformation (4.3) enables one to transform away most of the terms in the Taylor expansion of $g(x, \lambda)$ about the singularity $(0, 0)$, but at the price of not automatically preserving the

stability properties of the zeros of g (i.e., the steady state solutions) even when c_1, c_2, c_3 are all chosen to be positive. All the terms that can be transformed away will be called removable terms; those remaining constitute the *normal form* $n(x, \lambda)$ of $g(x, \lambda)$ near the singularity $(0,0)$. Thus, the normal form n satisfies

$$g(x, \lambda) \underset{\Gamma}{\approx} n(x, \lambda) \underset{\Gamma}{\approx} n(x, \lambda) + p(x, \lambda), \quad (4.4)$$

where $p(x, \lambda)$ is any removable term. In addition, one can find a *universal unfolding* of this singularity, $n(x, \lambda, \alpha)$, where $\alpha \in \mathbb{R}^k$ are unfolding parameters, such that

$$n(x, \lambda, 0) = n(x, \lambda),$$

and

$$n(x, \lambda) + q(x, \lambda) \underset{\Gamma}{\approx} n(x, \lambda, \alpha), \quad (4.5)$$

where $q(x, \lambda)$ is any Γ -symmetric perturbation. Physically, this states that perturbations of a system that respects the symmetry group Γ are subsumed in the normal form by the addition of extra terms whose coefficients (the unfolding parameters) vanish in the unperturbed system. The theory described above is discussed in detail by Golubitsky and Schaeffer [11].

For the problem with the midplane reflection symmetry Swift [12] finds that, after an appropriate rescaling,

$$n_1(z, \lambda) = z_1(-\lambda + a\sigma_1 + u_1 + d\sigma_1^2) \pm q\bar{z}_2\bar{z}_3, \quad (4.6)$$

provided

$$a + 1 \neq 0, \quad 2a + 1 \neq 0, \quad 3a + 1 \neq 0. \quad (4.7)$$

It is also assumed that the coefficients of $\lambda z_1, u_1 z_1$ and $q\bar{z}_2\bar{z}_3$ do not vanish. The signs of the first two can be fixed by an appropriate choice of c_1 and c_3 in the transformation (4.3). Observe that the nor-

mal form (4.6) is the right side of (3.10) with one extra term, and that the nondegeneracy conditions are those listed in theorem 1. The universal unfolding of this form is

$$\tilde{n}_1(z, \lambda) = z_1(-\lambda + \bar{a}\sigma_1 + u_1 + \bar{d}\sigma_1^2) \pm q\bar{z}_2\bar{z}_3, \quad (4.8)$$

where \bar{a}, \bar{d} are close to a, d . The coefficients a, d are called modal parameters. Although the bifurcation diagrams obtained from (4.8) are Γ_s -inequivalent for different choices of (a, d) , they are topologically equivalent within a range of parameter values (cf. section 3). The stability assignments for the four bifurcating branches can be shown to be invariants of Γ_s -equivalence, and are described in section 3. In this case therefore, both methods provide identical and complete descriptions of the bifurcation problem.

The normal form the problem without the midplane reflection symmetry is quite different. If we write

$$g_1(z, \lambda) = z_1(h_{1,\lambda}(0)\lambda + h_{1,\sigma_1}(0)\sigma_1 + h_3(0)u_1 + \dots) + p_2(0)\bar{z}_2\bar{z}_3 + \dots \quad (4.9)$$

In eq. (2.6), then the scaled normal form becomes

$$n_1(z, \lambda) = z_1(-\lambda + u_1) + \bar{z}_2\bar{z}_3, \quad (4.10)$$

with the nondegeneracy conditions

$$h_{1,\lambda}(0) \neq 0, \quad h_{1,\sigma_1}(0) + h_3(0) \neq 0, \quad p_2(0) \neq 0. \quad (4.11)$$

Note that in contrast to (4.6) all the signs can be fixed by choosing c_1, c_2, c_3 in eq. (4.3). However, changing the sign of c_2 changes H^+ to H^- . This result may be obtained by the methods of section 3 (together with a near identity coordinate change in the amplitude equation (2.6)) or by singularity theory methods. The only solutions near the origin ($z = 0, \lambda = 0$) are rolls and hexagons. This follows from the fact that the only two maximal isotropy subgroups of Γ_n are those corresponding to rolls and hexagons (fig. 3), and the fact that the dimension of the fixed point set F_z for these solutions is

one (see section 2). This guarantees the existence of two branches, one of rolls and the other of hexagons, bifurcating off the trivial solution at $\lambda = 0$. Moreover, it is easy to show that there are no other solutions near the origin. The normal form (4.10) admits the two solutions

Rolls: $\lambda = \sigma_1$,
 Hexagons: $\lambda = x + x^2$,

where we have parametrized the hexagons by $x = x_1 = x_2 = x_3 \neq 0$, with $x > 0$ for H^+ and $x < 0$ for H^- . Since $\sigma_1 = 3x^2$ along hexagons,

$$\lambda = \pm \sqrt{\sigma_1/3} + \sigma_1/3, \text{ for } H^\pm. \tag{4.12}$$

The appropriate bifurcation diagrams and stability assignments are shown in fig. 7 (cf. [1]).

Note that in this case there are no stable non-trivial solutions near the onset of convection. This unsatisfactory feature of the normal form (4.10) can be removed by choosing parameters that make the quadratic term in the normal form small. In this case, the bifurcation analysis will be able to capture the turning over of the unstable branch of the H^+ hexagons. At the turning point, stable solutions appear via a saddle-node bifurcation. In the language of singularity theory we seek an *organizing center*. This is a point in parameter

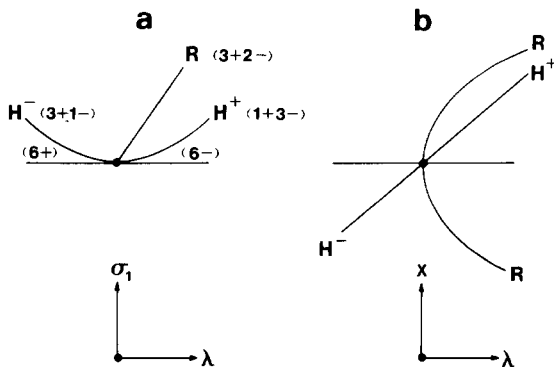


Fig. 7. Bifurcation diagrams for the nondegenerate problem without the midplane reflection symmetry computed from eq. (4.12) in (a) the σ_1 - λ plane, and (b) in the x - λ plane. There are no stable solutions.

space at which the bifurcation is *degenerate* ($p_2(0) = 0$, in the present example) with the property that the *universal unfolding* of the normal form for this degenerate bifurcation captures “all” the steady state bifurcation behavior of the problem.

In the present case, the quadratic term vanishes whenever the linear stability problem is selfadjoint. The normal form for this degenerate bifurcation is

$$n_1 = z_1(-\lambda + a\sigma_1 + u_1 + d\sigma_1^2) + \bar{z}_2\bar{z}_3(b\sigma_1 + u_1 + cq), \tag{4.13}$$

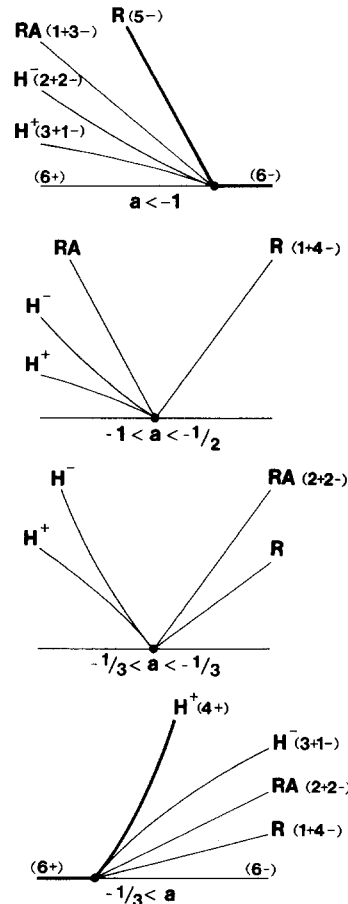


Fig. 8. Bifurcation diagrams for the degenerate problem ($\epsilon = 0$) without the midplane reflection symmetry computed from eq. (4.13) for $3b + 1 < 0$. The sign of $(3b + 1)$ determines one eigenvalue of the hexagon solutions and their relative amplitudes. For $3b + 1 > 0$ the labels “ H^+ ” and “ H^- ” are interchanged.

provided that the coefficients of λz_1 , $z_1 u_1$ and $\bar{z}_2 \bar{z}_3 u_1$ do not vanish, and

$$a + 1 \neq 0, \quad 2a + 1 \neq 0, \quad 3a + 1 \neq 0, \quad c \neq 0, \quad 3b + 1 \neq 0. \quad (4.14)$$

Observe that (4.13) differs from the normal form (3.10) for the symmetric bifurcation in having nonzero quartic terms. The appropriate universal unfolding (i.e., the normal form for a vector field that is close to the above) is found to be

$$n_1 = z_1(-\lambda + \tilde{a}\sigma_1 + u_1 + \tilde{d}\sigma_1^2) + \bar{z}_2 \bar{z}_3(-\epsilon + \tilde{b}\sigma_1 + u_1 + \tilde{c}q), \quad (4.15)$$

where the unfolding parameter ϵ is small, and \tilde{a} , \tilde{b} , \tilde{c} , \tilde{d} are close to the values a , b , c , d computed at the degenerate bifurcation ($\epsilon = 0$). As long as the nondegeneracy conditions (4.14) are met then the slight perturbation of a to \tilde{a} , etc., does not result in topologically different bifurcation diagrams.

The bifurcation diagrams for $\epsilon = 0$ are shown in fig. 8. The diagrams are drawn accurately for the

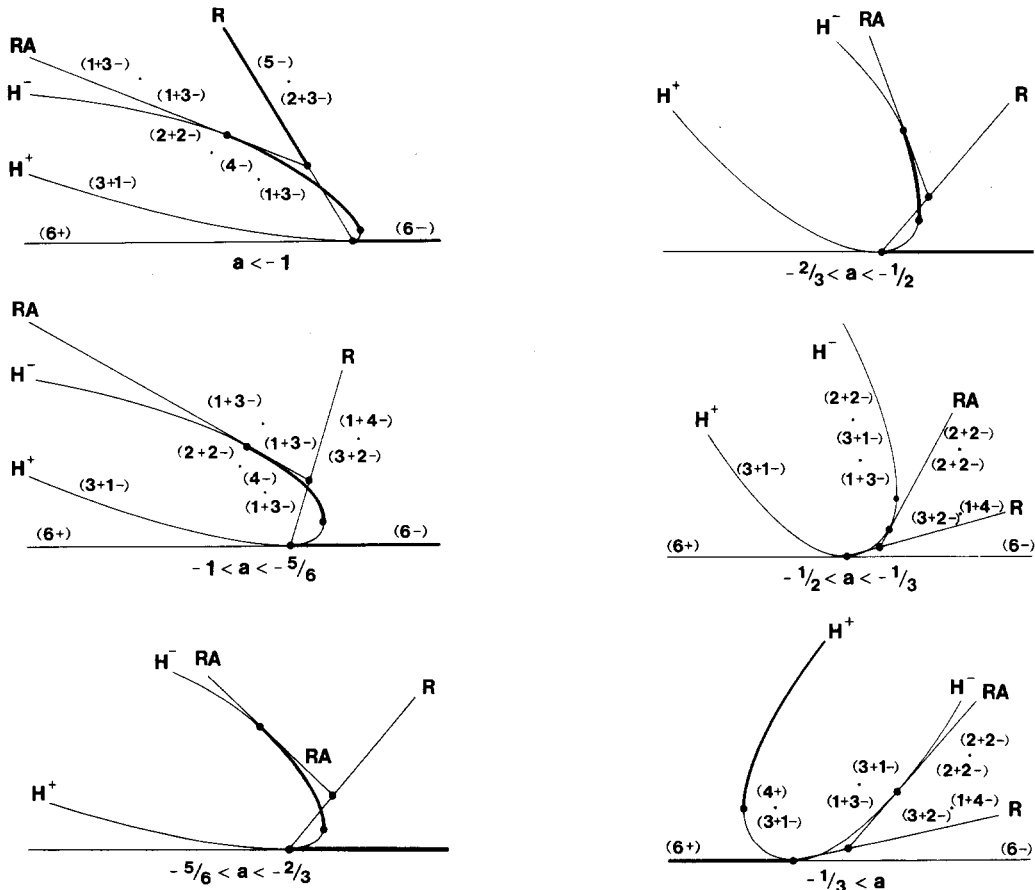


Fig. 9. Unfolding of the degenerate bifurcation diagrams of fig. 8 obtained by adding a small quadratic term ($\epsilon \neq 0$) to eq. (4.13). The diagrams are drawn for $\epsilon > 0$, $3b + 1 < 0$ and $d = 0$. See fig. 10 for other cases. The signs of the eigenvalues are shown for each arc of the solution branch between secondary bifurcations, indicated by dots. Additional crossings of the solutions branches are artifacts of the projection of the three complex amplitudes onto the σ_1 -axis. The ordering in λ of the secondary bifurcations for $-1 < a < -\frac{1}{2}$ can differ as illustrated, but the eigenvalues are unchanged.

case $d = 0$; the effect of $d \neq 0$ becomes insignificant, and the separation between the two hexagon branches vanishes as one looks closer and closer to the origin.

When ϵ is small but nonzero there are many more cases to consider. The possible bifurcation diagrams are shown in figs. 9 and 10. Fig. 9 shows the secondary bifurcations involving the rectangle solutions, which occur at $\lambda, \sigma_1 = \mathcal{O}(\epsilon^2)$. Fig. 10 shows that the two hexagon branches may undergo secondary bifurcations at larger amplitudes, i.e., $\lambda = \mathcal{O}(\epsilon)$. The figure shows only the equal amplitude branches, hexagons and triangles; rolls and rectangles need not be included since for these

solutions fig. 9 remains qualitatively correct even at these larger amplitudes.

Tables V and VI give the data needed to draw the bifurcation diagrams. The rectangle branch is nearly linear in the $\lambda\sigma_1$ plane; the main effect of adding the quadratic term (i.e., $\epsilon \neq 0$), is to change the point (σ_1^*, λ^*) where the branch bifurcates off the branch of rolls, but not its slope.

The secondary bifurcation at (σ_1^*, λ^*) is a pitchfork of revolution, i.e., a nondegenerate bifur-

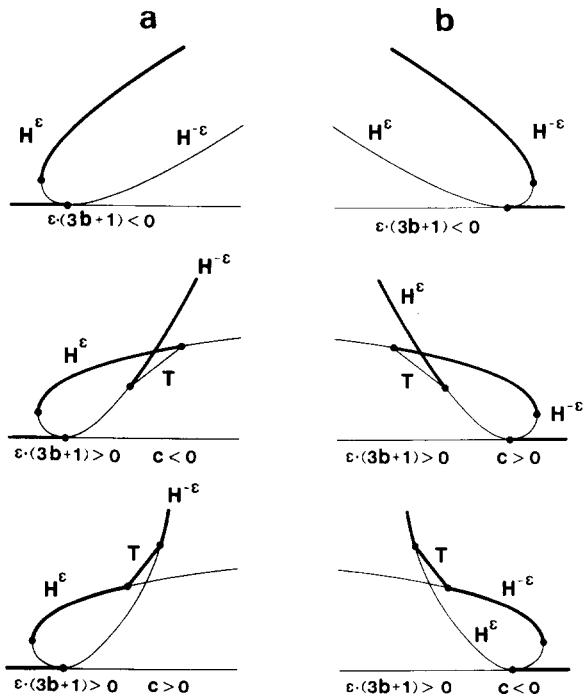


Fig. 10. Bifurcation diagrams for the unfolded degenerate D_3 normal form (4.16), with $a > -\frac{1}{3}$ (fig. 10a) and $a < -\frac{1}{3}$ (fig. 10b). The notation H^ϵ indicates H^+ or H^- depending on $\text{sgn}(\epsilon)$. Heavy lines indicate possible stable solutions, with eigenvalues $(2+)$ in fig. a and $(2-)$ in fig. b. Light lines indicate $(1+1-)$ for H^\pm and T, and $(2-)$ or $(2+)$ for the trivial solutions in fig. a, b, respectively. These diagrams complete fig. 9, showing the large amplitude ($\lambda = \mathcal{O}(\epsilon)$) behavior of the hexagon and triangle solutions. In this context two positive eigenvalues are added.

Table V
Data for solution branches

II. (R)	$\lambda = (a + 1)\sigma_1 + d\sigma_1^2$
III. (H)	$\lambda = -\epsilon x + (3a + 1)x^2 + (3b + 1)x^3 + (9d + 2c)x^4$ where $\sigma_1 = 3x^2, x > 0$ for $H^+, x < 0$ for H^- .
IV. (RA)	$\lambda - \lambda^* = (a + \frac{1}{2})(\sigma_1 - \sigma_1^*) + \dots$, where $\sigma_1^* = \epsilon^2 + \mathcal{O}(\epsilon^3), \lambda^* = (a + 1)\epsilon^2 + \mathcal{O}(\epsilon^3)$. $\left(\frac{1}{A}\right)^2 = \frac{\epsilon + x - bx^2}{2bx^2 + 2cx^3}, \sigma_1 = (1 + A^2)x^2$, where $x_1 \equiv x = Ax_2 = Ax_3$.
V. (T)	$\lambda = (a + \frac{1}{3})\sigma_1 + d\sigma_1^2$ $\cos \Phi = \frac{\sqrt{3}}{2c} (3\epsilon - (3b + 1)\sigma_1)\sigma_1^{-3/2}$.

Table VI
Summary of secondary bifurcation data

R/RA	bifurcation (pitchfork of revolution) $\sigma_1 = \epsilon^2 + \mathcal{O}(\epsilon^3)$ $\lambda = (a + 1)\epsilon^2 + \mathcal{O}(\epsilon^3)$
H/RA	bifurcation (Transcritical, D_3 symmetry) $x = -\epsilon + \mathcal{O}(\epsilon^2), \sigma_1 = 3x^2$ $\lambda = (3a + 2)\epsilon^2 + \mathcal{O}(\epsilon^3)$
H	bifurcation (saddle-node) $x = \frac{\epsilon}{2(3a + 1)} + \mathcal{O}(\epsilon^2)$ $\lambda = -\frac{1}{4} \frac{\epsilon^2}{(3a + 1)} + \mathcal{O}(\epsilon^3)$
H^\pm/T	bifurcation (Pitchfork) (occurs only if $\epsilon(3b + 1) > 0$) $\sigma_1 = \frac{3}{3b + 1} \left[\epsilon \mp 2c \left(\frac{\epsilon}{3b + 1} \right)^{3/2} \right] + \mathcal{O}(\epsilon^2)$ $\lambda = \frac{3a + 1}{3b + 1} \left[\epsilon \mp 2c \left(\frac{\epsilon}{3b + 1} \right)^{3/2} \right] + \mathcal{O}(\epsilon^2)$

cation with $O(2)$ symmetry. To understand this, note that the rectangle solutions near the bifurcation are of the form $z = (a, be^{-it}, be^{it})$, where $|b/a| = |A^{-1}| \ll 1$. The parameter t is the “angle” of the $O(2)$ rotation/reflection symmetry, and corresponds to a translation of the rectangle along the roll axis. At the bifurcation two eigenvalues of the rolls change sign.

The secondary bifurcation involving the hexagons and rectangles is more subtle. Three rectangles with $A \approx 1$ (or $A \approx -1$) collide with the hexagon branch in a bifurcation with D_3 symmetry. Two eigenvalues of the hexagons change sign at the bifurcation, while the rectangles have no net change in the number of positive and negative eigenvalues. An example of transcritical bifurcation with D_3 symmetry is given by the flow diagram for the triangles near $\Phi = \pi/2$ (cf. fig. 5), where four stagnation points of the flows coalesce at $\Phi = \pi/2$.

The secondary bifurcations involving hexagons and triangles (fig. 10) can be studied by restricting g to the 2-dimensional fixed point set of the triangles, $z(1, 1, 1)$, with $z \in \mathbb{C}$. The normal form (4.15) restricted to the equal amplitude solutions is

$$n|_{F_{D_3}} = z(-\lambda + (3a + 1)u + 9du^2) + \bar{z}^2(-\epsilon + (3b + 1)u + cq), \quad (4.16)$$

where $u = u_\alpha$, $z = z_\alpha$ ($\alpha = 1, 2, 3$), and $q = z^3 + \bar{z}^3$. This equation has the symmetries $z \mapsto \bar{z}$ and $z \mapsto \exp(2\pi i/3)z$. These are the symmetries of a triangle in the complex plane. In fact, it can be shown, though we shall not do so here, that any g with the Γ_n symmetry (cf. eq. (2.6)), restricted to the equal amplitude solution has D_3 symmetry, i.e., $h = g|_{F_{D_3}}$ commutes with D_3 . When $\epsilon = 0$, eq. (4.16) is D_3 -equivalent to the degenerate normal form with D_3 symmetry computed by Golubitsky and Schaeffer [13]. The universal unfolding is given by letting $\epsilon \neq 0$.

If $\epsilon(3b + 1) < 0$, there are no triangle solutions at small amplitudes and fig. 9 is complete. If $\epsilon(3b + 1) > 0$ there is a branch of triangles connecting the two hexagon branches at $\lambda = O(\epsilon)$, as

shown in fig. 10. The transition between the two hexagon branches can be either gradual or hysteretic depending on the stability of the triangle branch. The triangles are created and destroyed via pitchfork bifurcations in the Φ -direction.

We are now in a position to describe the relation between the results of the calculations with and without the midplane reflection symmetry. The midplane reflection symmetry is never exactly satisfied in convection since the Boussinesq approximation is not exact. It is important therefore to consider the effect of adding small symmetry breaking terms to the Γ_s amplitude equations. In general, we expect all even order terms to appear when the symmetry is broken, although typically the quadratic term is the most important. The bifurcation diagrams that one obtains depend in an essential way on the relative magnitude of the quadratic and quartic terms. In the remainder of this section we describe what happens when the coefficients of *both* terms are *small* (i.e. perturbed away from zero). This situation is expected to occur when the symmetry is broken only slightly, for example, because of slight differences in the thermal conductivity of the top and bottom boundaries. In this case certain secondary bifurcations involving hexagons and triangles can occur near the origin that are not present in the analysis of Buzano and Golubitsky. This is because Buzano and Golubitsky consider, in consequence of their nondegeneracy conditions, the case where the coefficients of the quartic terms are not small. Then the degenerate bifurcation with no quadratic term is described by the normal form (4.13) with the corresponding bifurcation diagrams in fig. 8, and the unfolded bifurcation (with a *small* quadratic term) is described by (4.15) and fig. 9. If we compare the results in fig. 8 with those for the symmetric case (fig. 6) we see that the addition of the quartic terms leaves the rolls virtually unchanged, while changing the patchwork quilt to a general rectangle (with $|A| \ll 1$). By contrast, the regular triangles present in the Γ_s problem (fig. 6) are eliminated when the fourth order terms are added: there are no triangles at all in fig. 8, only

hexagons. In order to understand what happens to the triangle branch it is necessary to consider the case in which the coefficients of the quartic terms are also *small*. This is done below for the equal amplitude solutions (H^\pm, T) for which the effects of symmetry breaking are most pronounced.

For the equal amplitude solutions it is possible to give a complete analysis of symmetry breaking using the methods of singularity theory. We have computed the normal form with the D_3 symmetry under the assumption that the even order terms are zero. The result is

$$n = z(-\lambda + (3a + 1)u) + c\bar{z}^2q, \quad (4.17)$$

where $c = \pm 1$ and $3a + 1$ can be scaled to be ± 1 . Eq. (4.17) is also the least degenerate normal form for the D_3 problem with an extra $z \mapsto -z$ symmetry, i.e., for $D_3 + Z_2 = D_6$. The universal unfolding of (4.17) is

$$\bar{n} = z(-\lambda + (3a + 1)u + Aq) + \bar{z}^2(-\epsilon + 3Bu + cq), \quad (4.18)$$

where ϵ, A and B are the unfolding parameters. We have thus embedded the symmetric normal form (4.17) in a structurally stable family of normal forms (4.18) without the symmetry. It is in this sense that our description of symmetry breaking for the problem with $D_3 + Z_2$ symmetry is complete. The parameter B replaces $b + \frac{1}{3}$ in eq. (4.16). The term Azq does not appear in (4.16); a nondegeneracy condition in the quartic terms enables one to transform it away by a Γ_n -equivalence (cf. [1]). In the present case we are perturbing a $D_3 + Z_2$ symmetric problem, containing no even terms rather than a degenerate ($\epsilon = 0$) nonsymmetric problem. The nondegeneracy condition therefore fails.

The bifurcation diagrams for (4.18) can be computed with the unfolding parameter A set equal to zero: A is a topologically trivial parameter. The results are shown in fig. 11 as a function of the remaining parameters ϵ and B . These diagrams replace fig. 10 when the midplane reflection sym-

metry is slightly broken. In contrast, fig. 9 remains virtually unchanged. Fig. 11 shows the various possible transitions, as λ is increased, involving the hexagons and triangles for the specific choices $a > -\frac{1}{3}$ and $C = \pm 1$. All of the secondary bifurcations involving the triangles are pitchforks in the phase variable Φ . The other cases ($a < -1/3$) are similar. Note that for larger amplitudes the broken symmetry diagrams in figs. 9 and 11 have a branch of rolls, a branch of rectangles, and two of hexagons. These, and their stability assignments, are in direct correspondence with the solutions of the Γ_s bifurcation diagram (fig. 6). Therefore, if the symmetry breaking is small, and we do not look too close to the origin, then the Γ_s results are a valid approximation. We see, as expected, that the quadratic term usually dominates the symmetry breaking effects as in regions 1 and 3 of fig. 11. However, if the fourth order perturbation is much larger than the quadratic term, then a different bifurcation diagram is appropriate, as in regions 2 and 4 of fig. 11. This happens when the symmetry breaking mechanism almost preserves the self-adjointness of the linear problem. On the other hand, self-adjoint problems with a large asymmetry in the boundary conditions are described by the bifurcation diagrams shown in fig. 8.

From a technical point of view, the situation involving the rectangles is rather more involved. This is because we do not get a complete description of symmetry breaking by restricting the amplitude equations for the symmetric case to the rectangle solutions, and unfolding the resulting degenerate normal form as we did above for the triangles. We are prevented from this by the presence of hidden symmetries (cf. [14]). If however, we consider the difference between the patchwork quilt and general rectangles as insignificant, then only the quadratic term is important for symmetry breaking. It is this term alone that pulls the rectangle branch way from the origin in fig. 9.

In order to have a rigorous theory of symmetry breaking from Γ_s to Γ_n , we would have to show that the normal form (4.6) found by Swift [12] for Γ_s -symmetric problem has a Γ_n -universal un-

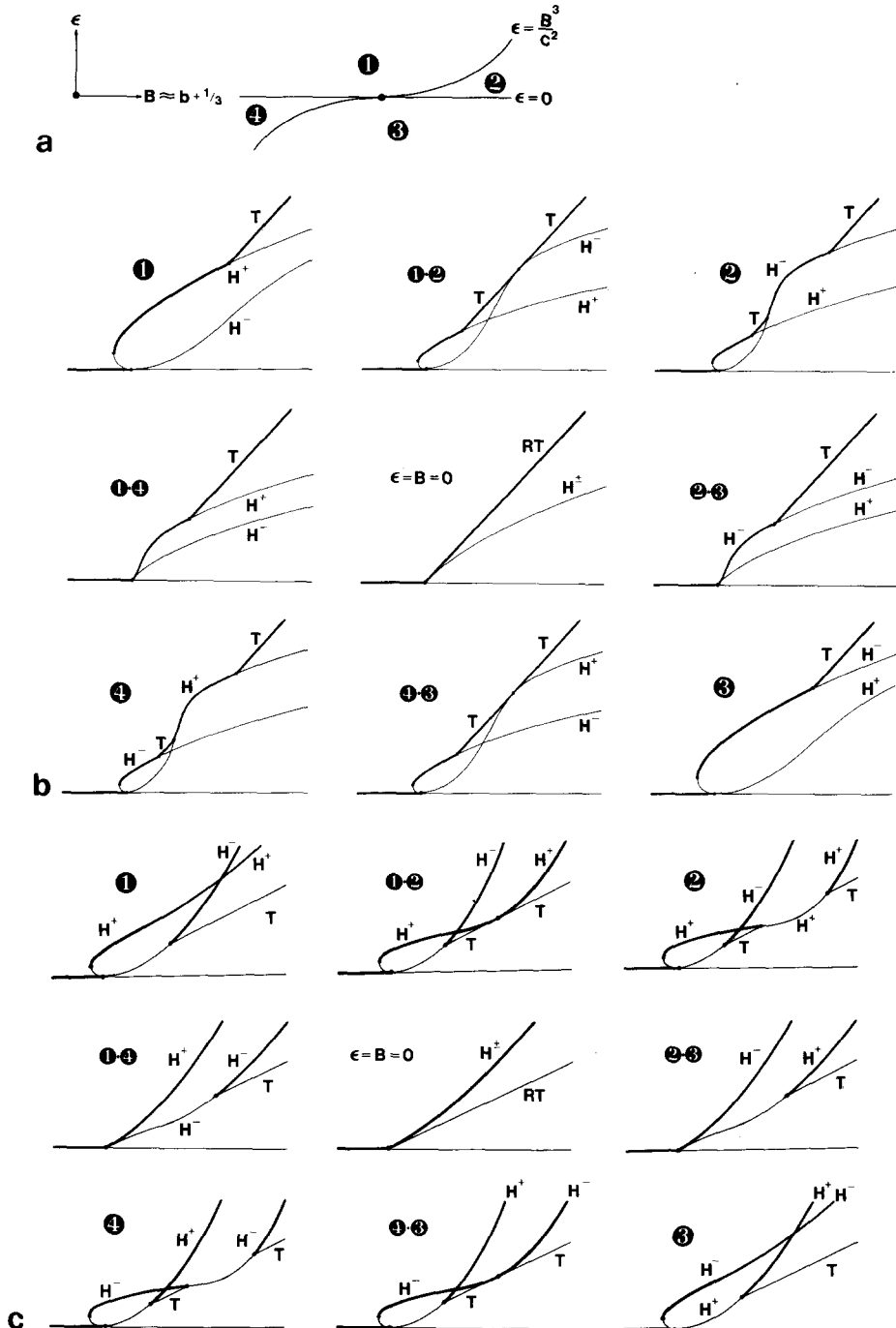


Fig. 11. Symmetry breaking of the equal amplitude solutions H^\pm , T as described by normal form (4.18) for $a > -\frac{1}{3}$ and $A = 0$, with $c = 1$ (fig. 11b) and $c = -1$ (fig. 11c). The ϵ - B plane (fig. 11a) divides into four regions; the bifurcation diagrams are drawn for each region and the boundaries. The other two cases ($a < -\frac{1}{3}$) are similar. Heavy lines indicate branches with two positive eigenvalues; light lines indicate (1 + 1 -) for H^\pm or T and (2 -) for the trivial solutions. The diagrams provide a complete description of symmetry breaking from the group $D_3 + Z_2$ to the group D_3 . Note that the large amplitude behavior is consistent with fig. 6, while the small amplitude behavior is consistent with fig. 10.

folding. Such a computation is theoretically possible using the result of Buzano and Golubitsky [1]. However, the calculations involved would be difficult and we have not attempted them. Our computation of the normal form with $D_3 + Z_2$ symmetry (4.17) and its universal unfolding in the D_3 symmetry (4.18) does give a lower bound on the complexity involved in breaking symmetry from Γ_s to Γ_n .

Our results show that the simplest possible way to break the symmetry of the normal form (4.8) is to use the unfolding

$$n_1 = z_1(-\lambda + a\sigma_1 + u_1 + d\sigma_1^2 + \alpha q) + \bar{z}_2\bar{z}_3(-\epsilon + \beta\sigma_1 + \gamma u_1 + cq), \quad (4.19)$$

where α , β , γ and ϵ are unfolding parameters. We have argued that only ϵ and $B = \beta + \gamma/3$ (cf. figs. 9 and 11) are important as far as the bifurcation diagrams are concerned.

5. Discussion

In this section we discuss our results in a broader context and relate them to experimental observations. The motivation for the present study was provided by our desire to understand clearly under what conditions hexagons or rolls should be expected near the onset of convection. This problem becomes tractable if the fluid layer is assumed to be infinite in both horizontal directions and the pattern assumed to be equivariant with respect to the group that preserves the hexagonal lattice. Both rolls and hexagons, as well as other solutions, fit on this lattice. We distinguished between two cases: the symmetric in which in addition the layer possesses a reflectional symmetry about the horizontal midplane and the nonsymmetric. In conjunction with the work of Buzano and Golubitsky, we have obtained a complete classification of the possible nondegenerate bifurcations of steady state solutions off the trivial state $z = 0$ in both cases. Our analysis highlights the extent to which the symmetry determines the possible bifurcation dia-

grams. The solutions that occur nearest the trivial state are those with maximal isotropy subgroups (i.e., the most symmetric nontrivial solutions), lending support to the conjecture [10] that this is a general result. We have not, however, addressed the question of which of the possible bifurcation diagrams applies to a given situation. This depends on the signs of certain terms and the values of a small number of modal parameters that enter in the normal form and that have to be computed for each specific problem. In this section we describe how symmetry can be used to learn a great deal about a physical system.

In convection problems with the extra reflectional symmetry, we have found that either rolls, regular triangles or hexagons could be stable near the bifurcation. The symmetry applies in systems with identical boundary conditions at the top and bottom, and constant fluid properties. Schlüter, Lortz and Busse [3] show that the modal parameter $a < -1$ for both free-free and rigid-rigid boundaries, and for all values of the Prandtl number, and conclude that rolls are the stable convection pattern near threshold. This has also been shown in a certain limiting case to be true for convection in a uniform vertical magnetic field with rigid-rigid boundaries [15]. Our analysis shows that in other circumstances (e.g. a different regime of magnetoconvection or doubly-diffusive convection) hexagons or regular triangles rather than rolls could be the stable convection pattern near threshold, even in the symmetric case. In this case, however, there would be no difference between H^+ and H^- ; the realized pattern would depend on initial conditions.

For problems that lack the reflectional symmetry we must distinguish between selfadjoint and non-selfadjoint problems. For example, convection between one rigid and one free (but undeformable) boundary with constant fluid properties [3] or convection between undeformable free-free or rigid-rigid boundaries with a y -dependent (but not temperature-dependent) viscosity [16] both lead to self-adjoint problems. It can be shown [3] that for such problems the quadratic term in the normal

form vanishes, and the preferred solution is then determined by the cubic terms. These self-adjoint but non-symmetric cases correspond to the degenerate normal form of Buzano and Golubitsky (eq. (4.13) and fig. 8). Small non-selfadjoint perturbations are described by the unfolded normal form (eq. (4.15) and figs. 9 and 10).

Non-selfadjoint problems arise naturally in a wide range of circumstances. This is because they are the least "special". We list below a number of effects that have been discussed in the literature and that give rise to non-selfadjoint problems ($\epsilon \neq 0$):

- a) the upper surface of the fluid is free to be deformed by the convection flow (Davis and Segel [17]);
- b) temperature-dependent surface tension effects are present (Scanlon and Segel [18]);
- c) the viscosity is temperature-dependent (Palm [19]);
- d) the thermal diffusivity is y -dependent (Palm [16]);
- e) the isobaric thermal expansion coefficient and heat capacity are temperature-dependent (Busse [20]);
- f) the heating is time-dependent (Krishnamurti [2], [21]);
- g) the density of the fluid depends quadratically on the temperature, as for example, in water near 4°C. (Veronis [22], Dubois et al. [23]), or liquid helium I near 2.178 K (Walden and Ahlers [24]).

If these non-selfadjoint effects are large, the results of eq. (4.10) and fig. 7 are appropriate, and the stable nontrivial solutions of the problem are inaccessible to perturbation theory. For small departures from self-adjointness there are two cases to consider, either the unperturbed problem is symmetric or it is not. For small departures from symmetry all of the even order terms are small, and figs. 9 and 11 are appropriate. Note that a symmetric problem is always self-adjoint. When $a > -\frac{1}{3}$ the observed behavior will typically be that located in regions 1 and 3 of figs. 11 a, b, i.e., the quadratic term dominates unless the perturbed problem remains close to being selfadjoint. In this

case the problem can exhibit the exotic behavior located in the thin wedges 2, 4 in fig. 11. Observe that only when $a > -\frac{1}{3}$ are there observable differences in the bifurcation diagrams (i.e., in the stable branches) between symmetry breaking while maintaining self-adjointness ($\epsilon = 0$), and more general symmetry breaking ($\epsilon \neq 0$).

For Bénard convection with rigid boundaries, a ranges smoothly from $-1.09 \dots$ for $P \rightarrow 0$ to $-3.40 \dots$ for $P \rightarrow \infty$ [3], so the case $a < -1$ is of particular interest. Fig. 9 shows subcritical instabilities to either H^+ or H^- , a region of hysteresis where rolls and hexagons can both be stable, and a secondary bifurcation by which the hexagons lose stability to rolls as the Rayleigh number is increased. Note that this completes the picture computed by Busse [20]. To a certain extent a bifurcation diagram of this type has been verified experimentally. Hexagons have been observed near threshold in cases (b), (c) and (f) above. Indeed, it has long been recognized that the hexagons observed in Bénard's original experiment were the result of surface tension effects [25]. In the problem with a temperature-dependent viscosity ν it has been shown ([19, 26, 27]) that if $dv/dT < 0$ as in liquids then H^+ hexagons (i.e., l -hexagons) are preferred at onset, while if $dv/dT > 0$ as in gases then the H^- hexagons (i.e., g -hexagons) are preferred. Thus, ϵ is proportional to dv/dT . In the experiments of Hoard et al. [28] on a fluid with a highly temperature-dependent viscosity hexagons were found near threshold whenever the layer depth was sufficiently small, but the hexagons persisted until $R = 3R_c$ where the experiment was terminated without finding the secondary transition to rolls. The experiments of Silveston [29] on large aspect ratio convection in silicon oil, do, however, provide some visual evidence for such a transition (see also Somerscales and Dougherty [30]). More recently, much more sophisticated experiments have been carried out on convection in liquid helium. In these experiments the conditions of the experiment can be controlled to a much greater precision; their only disadvantage is that the flow pattern cannot be visualized, and con-

vective transitions can be detected only in so far as they affect a global quantity like the convective heat transport (the Nusselt number). The experiments of Walden and Ahlers [24] on large aspect ratio convection in liquid helium I near 2.178 K, the temperature at which the density is maximum (case (g) above), are the most complete. These experiments reveal a hysteretic transition very near the onset of convection which may be identified with the subcritical bifurcation to hexagons. A second hysteresis loop observed at values of R greater than R_c may be identified with the transition from hexagons to rolls as R is increased. These observations are in qualitative agreement with the predictions by Busse [20].

We have seen in detail the role played by the symmetries of the problem in determining the variety of possible bifurcation diagrams. Thus, Busse's calculation can be seen from the broader perspective of bifurcations in the presence of a symmetry group.

One disadvantage of our treatment is that stability is computed only within the hexagonal lattice. A pattern which is predicted here to be stable may be unstable to squares. Indeed, squares are observed in the salt finger regime of doubly diffusive convection [31].

Finally, it should be borne in mind that experiments are always affected to some extent by the presence of sidewalls. This effect, including the role of symmetry breaking in the horizontal that can be caused by the sidewalls, is beyond the scope of the present work.

Acknowledgements

This work was supported in part by the National Science Foundation under grants MCS 81-01580 (M.G.) and AST 79-23243 (E.K.), the California Space Institute under grants CS 4-81 and CS 42-82 (J.W.S. and E.K.), the Army Research Office under contract DAAG-29-79-C-0086 (M.G.) and the Alfred P. Sloan Foundation (E.K.). We would like to thank Fritz Busse, John Guckenheimer, Jerry Marsden and David Schaeffer for many helpful discussions.

References

- [1] E. Buzano and M. Golubitsky, *Phil. Trans. Roy. Soc. Lond. A* 308 (1983) 617-667.
- [2] R. Krishnamurti, *J. Fluid Mech.* 33 (1968) 457-463.
- [3] A. Schlüter, D. Lortz and F. H. Busse, *J. Fluid Mech.* 23 (1965) 129-144.
- [4] F.H. Busse, *Rep. Prog. Phys.* 41 (1978) 1929-1967.
- [5] J. Guckenheimer and P. Holmes, *Nonlinear Oscillations, Dynamical Systems and Bifurcations of Vector Fields*, Springer Series in Applied Mathematical Sciences v. 42, 1980.
- [6] D. Sattinger, *Group Theoretic Methods in Bifurcation Theory* (Springer, New York, 1975) (Lecture Notes in Mathematics vol. 762).
- [7] E.L. Koschmieder, *Adv. Chem. Phys.* 26 (1974) 177-188.
- [8] J.E. Marsden and M. McCracken, *The Hopf Bifurcation and Applications* (Springer New York, 1976) (Applied Mathematical Sciences, vol 19).
- [9] S. Chandrasekhar, *Hydrodynamic and Hydromagnetic Stability* (Oxford Univ. Press, Oxford, 1961).
- [10] M. Golubitsky, *Bifurcation Theory, Mechanics and Physics*, C.P. Bruter et al. eds. (D. Reidel, Dordrecht, 1983) pp. 225-256.
- [11] See, for example M. Golubitsky and D. Schaeffer, *Commun. Math. Phys.* 67 (1979) 205-232; or M. Golubitsky and D. Schaeffer, *Commun. Math. Phys.* 67 (1979), 205-232; or M. Golubitsky, and D. Schaeffer, *Proc. Symposia in Pure Math.* 40, A.M.S. (1983) 499-515.
- [12] J.W. Swift, Ph.D Thesis, University of California, Berkeley, in preparation.
- [13] M. Golubitsky, and D. Schaeffer, *Commun. Pure Appl. Math.* 35 (1982) 81-111.
- [14] M. Golubitsky, J.E. Marsden and D. Schaeffer, *Partial Differential Equations and Dynamical Systems*, W. Fitzgibbon, ed. (Pitman, London, 1984), to appear.
- [15] F.H. Busse and R.M. Clever, *Phys. Fluids* 25 (1982) 931-935.
- [16] E. Palm, *Ann. Rev. Fluid Mech.* 7 (1975) 39-61.
- [17] S.H. Davis and L.A. Segel, *Phys. Fluids* 11 (1968) 470-476.
- [18] J.W. Scanlon and L.A. Segel, *J. Fluid Mech.* 30 (1967) 149-162.
- [19] E. Palm, *J. Fluid Mech.* 8 (1960) 183-192.
- [20] F.H. Busse, *J. Fluid Mech.* 30 (1967) 625-649.
- [21] R. Krishnamurti, *J. Fluid Mech.* 33 (1968) 445-455.
- [22] G. Veronis, *Astrophys. J.* 137 (1963) 641-663.
- [23] M. Dubois, P. Bergé and J. Wesfreid, *J. Phys.* 39 (1978) 1253-1257.
- [24] R.W. Walden and G. Ahlers, *J. Fluid Mech.* 109 (1981) 89-114.
- [25] M.J. Block, *Nature* 178 (1956) 650-651.
- [26] A. Graham, *Phil. Trans. Roy. Soc. A* 232 (1933) 285-296.
- [27] H. von Tippelskirch, *Beitr. Phys. Atmos.* 29 (1956) 37-54.
- [28] C.Q. Hoard, C.R. Robertson and A. Acrivos, *Int. J. Heat Mass Transfer* 13 (1970) 849-456.
- [29] P.L. Silveston, *Forsch. Ing. Wes.* 24 (1958) 59-69.
- [30] E.F.C. Somerscales and T.S. Dougherty, *J. Fluid Mech.* 42 (1970) 755-768.
- [31] T.G.L. Shirtcliffe and J.S. Turner, *J. Fluid Mech.* 41 (1970) 707-719.